Abstract

GENERAL, IGNACIO J. QCD Coulomb Gauge Approach to Exotic Hadrons. (Under the direction of Prof. Stephen R. Cotanch.)

The Coulomb Gauge Hamiltonian (CGH) model, a field theoretical, relativistic, many-body approach to Quantum Chromodynamics (QCD), is developed, which describes the vacuum through a Bogoliubov-Valatin transformation. This transformation also dresses the bare quarks and gluons, producing quasi-particles with constituent masses and quark and gluon condensates. This framework is then applied, using the variational principle, to the hybrid meson and tetra-quark problems, where exotic quantum numbers can be generated; light ($u\bar{u}g$), strange ($s\bar{s}g$) and charmed ($c\bar{c}g$) hybrid meson spectra are calculated and found to agree reasonably well with lattice and Flux Tube predictions. The light tetra-quark spectra is also calculated, along with the charmed tetra-quark structures likely to be the $X(3872)$ and $Y(4262)$ particles. The lowest 1^{-+} hybrid meson mass is found to be just above 2.2 GeV while the lightest tetraquark state mass with these exotic quantum numbers is predicted around 1.4 GeV. These theoretical formulations all indicate the observed 1^{-+} $\pi_1(1600)$ and, more clearly, $\pi_1(1400)$ are definitely not hybrid states but could be tetra-quark states, with a molecular type, meson-meson structure.

QCD Coulomb Gauge Approach to Exotic Hadrons

by

Ignacio J. General

A dissertation submitted to the Graduate Faculty of
North Carolina State University
in partial fulfillment of the
requirements for the Degree of
Doctor of Philosophy

Physics

Raleigh, December 2006

Approved by:

Prof. S. R. Cotanch Chair of Advisory Committee	Prof. D. Lee
Prof. A. Young	Prof. R. Fulp

a Josefina y Horacio, mis padres

(to Josefina and Horacio, my parents)

BIOGRAPHY

I was born in Buenos Aires, Argentina, in November of 1973. I grew up in downtown Buenos Aires, with all the noise and endless motion of this overwhelming and lovable city. There I attended Salvador School, a great Jesuit school, where, through the years, I learned the importance of knowledge but, more essentially, the importance of good friends.

When I finished school, I was very keen on two fields, computers and physics; economical considerations about my future inclined me to choose the former. But when I was about to register in college, I came across a physics talk which convinced me about my real passion. That is how I began studying physics, almost by chance.

I started my studies in Salvador University, in their new physics school. Unfortunately, after 3 years I realized the people in charge were not up to my expectations, with exception of a great professor, Enrique Cabanillas, who clearly transmitted the students his love for physics. Also, I can not regret the good friends I met there. So I moved on to Buenos Aires University, where I received my degree of "Licentiate in Physical Sciences". During those years, I married Eliana, also a physics student, who I had a beautiful baby with, Camila.

After a few years away from physics I decided to pursue a PhD, motivated by my friend Henry Herce. So, with my wife, we initiated our graduate studies at North Carolina State University, in Raleigh, North Carolina, USA. My research was developed under the advice of Professor Steve Cotanch, in hadron physics. I have spent about 4 years in this lovely and quiet city, with my wife and my two daughters, Camila and the North Carolinian, Clara.

I have to say that I will certainly miss this city and its kind people ...

ACKNOWLEDGMENTS

I wish to express my deep gratitude to my advisor, Steve Cotanch, for all his good guidance and support. Thanks to Felipe Llanes-Estrada, who helped me an infinite number of times, despite being far away in Spain; also, thanks for his warm reception when I travelled to the beautiful city of Madrid. Thanks to Ping Wang, for many enlightening discussions.

Thanks to the members of my committee, Professors Dean Lee and Albert Young.

Thanks to the Department of Physics at NCSU, especially to Prof. Michael Paesler, Jenny Allen and Rebecca Savage. Also thanks to Prof. Ronald Fulp, from the Department of Mathematics and member of my committee, for his wonderful lectures in Differential Geometry.

I would also like to thank my parents, for their constant love and support, for everything they ever did for me. Also, thanks to my brother, Federico, and the many good friends I encountered along my life, for helping me become who I am.

And lastly, thanks to my wife, Eliana, and my daughters, Camila and Clara, for they are a light in my life.

Contents

List of Tables

List of Figures

Yet nature is made better by no mean
But nature makes that mean: so, over that art
Which you say adds to nature, is an art
That nature makes.

William Shakespeare, *The Winter's Tale*, 4.4.79-103

Chapter 1

Introduction

Quantum Chromodynamics is a non-abelian quantum field theory that describes the strong interactions of quarks and gluons. QCD's success is fundamentally appreciated in the high energy regime, where scattering processes are calculated with great accuracy. This is due to a property of this theory, called asymptotic freedom, in which the interaction due to gluon exchange vanishes in the infinite momentum limit, allowing a perturbative expansion in the quark-gluon coupling constant. However, the low energy regime does not share this property, therefore it requires a non-perturbative approach. Thus, there is a complete Lagrangian, containing every dynamical aspect of the theory, but from which little information can be extracted regarding interesting physical processes. In particular, there is not much QCD insight into the properties of non-standard hadrons, such as glueballs, hybrids, tetra-quarks, penta-quarks and so on. Quark models successfully describe mesons and baryons, but not exotic particles, with quantum numbers not compatible with a structure of three quarks or a quark and an anti-quark. It is expected, and there is some experimental evidence, that such states exist, but little is known theoretically about them. The purpose of this dissertation is to address this issue.

As a consequence, several non-perturbative QCD methods have been developed. Perhaps, the most fundamental is "Lattice QCD", which attempts to numerically

solve QCD in a discrete space-time. However serious problems arise, such as the extrapolations needed to include light quarks or the inclusion of finite chemical potentials (1), requiring some approximations. Another option is to use effective theories (models), containing simplified Lagrangians with the same qualitative characteristics of QCD, e.g., its symmetries. An example is the "Nambu and Jona-Lasinio (NJL) model" (2; 3); its Lagrangian originally described a two-body (massless) nucleon interaction, with chiral symmetry, whose spontaneous rupture gives rise to a nucleon mass and generates a Goldstone boson, the pion. This model, when reinterpreted as describing a two-body quark interaction where the gluon degrees of freedom are frozen, can successfully describe many hadronic properties. Another useful and more intuitive model is the "Flux Tube" (4), where the quark pairs are connected by gluonic fields, forming a tube. It is a clear picture how confinement is realized in this model: when the quark and antiquark in a meson are separated, the tube is stretched until it is energetically favorable for it to break, generating two tubes, each with a quark-antiquark pair at the ends, i.e., two mesons.

In this thesis, some hadronic aspects are investigated using another model based on the Coulomb gauge Hamiltonian of QCD. This model has been successfully applied to the quark and gluon sectors in a series of publications (5; 6; 7; 8; 9; 10; 11). The model's Hamiltonian respects the global, internal symmetries of QCD, as well as the spatial Euclidean group, all within a minimal two parameter theory. It incorporates chiral symmetry, yet dynamically generates a constituent mass and spontaneously breaks chiral symmetry (6). The mechanism through which this occurs parallels that of the Bardeen, Cooper and Schrieffer (BCS) theory of superconductivity. Also, applying a Bogoliubov-Valatin (BV) transformation, non-linear gap equations, both for the quark (6) and gluon sectors (9), can be derived and solved to give vacuum properties, as its quasi-particles and condensates. Approximate diagonalizations of the Hamiltonian, via the Tamm-Dancoff (TDA) and Random Phase Approximation (RPA) treatments provide a reasonable description of the low energy u, d, s and

c meson spectra (8). Further, in the RPA, a Goldstone boson emerges which is identified with the pion. When applied to the gluon sector, the model is found to be consistent (11) with lattice glueball (and oddball) predictions. In particular, it provides a glueball Regge trajectory ($J^{PC} = 2^{++}$, 4^{++}) similar to the Pomeron diffraction fit. Also, the controversial odderon ($P = C = -1$) was studied in this context, predicting a trajectory subdominant to the pomeron which can explain its nonobservance in reactions with pomeron exchange. Finally, a hyperfine interaction (2^{nd} order correction to the Hamiltonian, previously neglected) can be incorporated, resulting in a realistic description of hadron spin splittings and a constituent quark mass comparable to that of phenomenological quark models (10).

This thesis is organized as follows: a brief account of QCD in the Coulomb gauge is given in next chapter, followed by the model specification in chapter 3. Then, the quasi-particle basis, along with its corresponding vacuum state and gap equations are discussed. The next two chapters address hybrid mesons and tetra-quarks. Finally, in chapter 7, the results are summarized and the conclusions of this work are discussed.

Chapter 2

Coulomb Gauge QCD Hamiltonian

2.1 Quantum Chromodynamics in the Coulomb Gauge

Quantum Chromodynamics is a non-abelian gauge theory that describes the strong interaction. Its degrees of freedom are given by fermionic (quarks) and gauge (gluons) fields. The former are defined by

$$\Psi(x) = \begin{pmatrix} u(x) \\ d(x) \\ s(x) \\ ... \end{pmatrix}, \tag{2.1}$$

where $u, d, s, ...$ represent flavor degrees of freedom, each of which can have any of three colors. Quark masses are expressed through a matrix,

$$m_0 = \begin{pmatrix} m_u & 0 & 0 & 0 \\ 0 & m_d & 0 & 0 \\ 0 & 0 & m_s & 0 \\ 0 & 0 & 0 & ... \end{pmatrix}. \tag{2.2}$$

The Lagrangian is then given by

$$\mathcal{L}_{QCD} = \overline{\Psi}\left(i\gamma_\mu D^\mu - m_0\right)\Psi - \frac{1}{4}F^a_{\mu\nu}F_a^{\mu\nu}, \tag{2.3}$$

where

$$D_\mu = \partial_\mu - igA_\mu \tag{2.4}$$

is the covariant derivative and $A_\mu = T_a A^a_\mu$ includes the gluonic fields A^a_μ (with color indices $a = 1, ..., 8$). Here, g is the coupling constant and T_a are the $SU_C\,(3)$ color group generators, given in appendix A. Finally,

$$F^a_{\mu\nu} = \partial_\mu A^a_\nu - \partial_\nu A^a_\mu + g f_{abc} A^b_\mu A^c_\nu \tag{2.5}$$

are the gluon field tensors (f_{abc} being the $SU_C\,(3)$ structure constants).

In order for the theory to be correctly defined, the gauge is fixed to $\nabla \cdot \mathbf{A} = \mathbf{0}$, the Coulomb gauge. With this choice, one can derive the Coulomb gauge QCD Hamiltonian (12; 13):

$$\begin{aligned}
H &= H_q + H_g + H_{qg} + H_C && (2.6)\\
H_q &= \int \Psi^\dagger(\boldsymbol{x})(-i\boldsymbol{\alpha}\cdot\boldsymbol{\nabla} + \beta m)\Psi(\boldsymbol{x})d\boldsymbol{x} && (2.7)\\
H_g &= \frac{1}{2}\int \left(\mathcal{J}^{-1}\mathbf{E}^a_{tr}\cdot\mathcal{J}\mathbf{E}^a_{tr} + \mathbf{B}^a\cdot\mathbf{B}^a\right)d\boldsymbol{x} && (2.8)\\
H_{qg} &= -g\int \mathbf{J}^a(\boldsymbol{x})\cdot\mathbf{A}^a(\boldsymbol{x})d\boldsymbol{x} && (2.9)\\
H_C &= \frac{1}{2}\int\int \mathcal{J}^{-1}\rho^a(\boldsymbol{x})K_{ab}(\boldsymbol{x},\boldsymbol{y})\mathcal{J}\rho^b(\boldsymbol{y})d\boldsymbol{x}d\boldsymbol{y}\ , && (2.10)
\end{aligned}$$

where $\rho^a(\mathbf{x}) = \Psi^\dagger(\boldsymbol{x})T^a\Psi(\boldsymbol{x}) - f^{abc}\mathbf{A}^b(\boldsymbol{x})\cdot\mathbf{E}^c_{tr}(\boldsymbol{x})$ and $\mathbf{J}^a = \Psi^\dagger(\boldsymbol{x})\boldsymbol{\alpha}T^a\Psi(\boldsymbol{x})$ are the color charge density and current, respectively, and $\mathbf{E}^a$ and $\mathbf{B}^a$ are the chromo-electric

and chromo-magnetic fields, defined in terms of the gluon fields by:

$$\mathbf{E}^a = -\dot{\mathbf{A}}^a - \boldsymbol{\nabla} A^{0a} + g f^{abc} A^{0b} \mathbf{A}^c \tag{2.11}$$

$$\mathbf{B}^a = \boldsymbol{\nabla} \times \mathbf{A}^a + \frac{1}{2} g f^{abc} \mathbf{A}^b \times \mathbf{A}^c; \tag{2.12}$$

the transverse part of the chromo-electric field is given by

$$\mathbf{E}^a_{tr} = -\dot{\mathbf{A}}^a - g(1 - \boldsymbol{\nabla}^{-2} \boldsymbol{\nabla} \boldsymbol{\nabla} \cdot) f^{abc} A^{0b} \mathbf{A}^c. \tag{2.13}$$

The kernel of the last integral in the Hamiltonian is given by

$$K_{ab}(\boldsymbol{x}, \boldsymbol{y}) = \langle \boldsymbol{x}, a | \frac{g}{\boldsymbol{\nabla} \cdot \boldsymbol{D}} (-\nabla^2) \frac{g}{\boldsymbol{\nabla} \cdot \boldsymbol{D}} | \boldsymbol{y}, b \rangle. \tag{2.14}$$

One way of deriving the Hamiltonian is by transforming from the gauge with $A^0 = 0$ to the Coulomb gauge and, as showed by Christ and Lee (13), this is similar to transforming from Cartesian to curvilinear coordinates, and generates a Jacobian, the Faddeev-Popov determinant $\mathcal{J} = det(\boldsymbol{\nabla} \cdot \boldsymbol{D})$.

The terms in the Hamiltonian describe, respectively, the kinetic energy of the quark fields, the kinetic energy and self-interaction of the glue, via the chromo-electric and chromo-magnetic fields, the minimal coupling of the quarks to the gauge fields, and, finally, the instantaneous Coulomb interaction.

2.2 Coulomb Gauge Hamiltonian Model

The rigorous QCD Hamiltonian has a series of complexities that make it impractical to directly diagonalize. Among these are the presence of the Faddeev-Popov determinant and the non-linearity introduced by the self-interactions of the non-abelian gluon fields (which result in 3 and 4 gluon vertices). In order to eliminate some of those difficulties, this work uses the CGH model, an effective Hamiltonian based on the Coulomb gauge Hamiltonian given in last section. The complexities mentioned above are partially

eliminated since the value of the Faddeev-Popov determinant is set to one, following (14), and the coupling constant is treated perturbatively, $\alpha_s \equiv \frac{g^2}{4\pi} < 1$. In this way, an adequate description of the high energy physics is obtained. To incorporate a correct hadron phenomenology (low energy regime), the instantaneous Coulomb interaction is suitably modeled. The effective Hamiltonian is:

$$
\begin{aligned}
H_{\text{eff}} &= H_q + H_g^{\text{eff}} + H_{qg} + H_C^{\text{eff}} && (2.15)\\
H_q &= \int d\boldsymbol{x}\Psi^\dagger(\boldsymbol{x})[-i\boldsymbol{\alpha}\cdot\boldsymbol{\nabla} + \beta m]\Psi(\boldsymbol{x}) && (2.16)\\
H_g^{\text{eff}} &= \frac{1}{2}\int d\boldsymbol{x}\,[\mathbf{E}^a_{tr}(\boldsymbol{x})\cdot\mathbf{E}^a_{tr}(\boldsymbol{x}) + \mathbf{B}^a(\boldsymbol{x})\cdot\mathbf{B}^a(\boldsymbol{x})] && (2.17)\\
H_{qg} &= -g\int d\boldsymbol{x}\ \mathbf{J}^a(\boldsymbol{x})\cdot\mathbf{A}^a(\boldsymbol{x}) && (2.18)\\
H_C^{\text{eff}} &= -\frac{1}{2}\int d\boldsymbol{x}d\boldsymbol{y}\rho^a(\boldsymbol{x})\hat{V}(|\boldsymbol{x}-\boldsymbol{y}|)\rho^a(\boldsymbol{y})\ , && (2.19)
\end{aligned}
$$

where $\hat{V}$ is an instantaneous kernel, further discussed in chapter 3.

Due to the above approximations the Coulomb gauge approach is not rigorous QCD but rather a model. However, approximate many-body diagonalizations of H_{eff} capture much of the QCD nature of hadrons and model predictions should provide a realistic description with fruitful structure insight. There are several reasons supporting this contention. First, the vacuum expectation value of the rigorous Coulomb kernel is known to have the shape of the Cornell potential from lattice studies (15). Second, it is known that confinement manifests itself in this kernel and not in transverse gluon exchange (the H_{qg} term) which is suppressed in the Coulomb gauge by an energy gap (for a recent account see (16)). Third, the connection between the gluon mass gap and the kernel used in this work is based on a simple gap equation where the cutoff plays the role of a dynamical mass counterterm. This treatment is consistent with $SU(2)$ lattice data (17) and is supported by an extended study (18) based on mean field theory and large N_c QCD. Fourth, the improved (dressed) quark and gluon degrees of freedom generated by the appropriate gap equations permit a

significantly truncated Fock state expansion involving quasi-quarks and quasi-gluons having mass gaps up to order 1 GeV. From energy considerations the dominant component of the Fock space expansion will therefore contain the minimum number of constituents possible and mixing with more complex Fock states, which have higher energies, will be suppressed. Fifth and final, the Faddeev-Popov determinant is set to 1, however its role is largely in enhancing the confinement interaction and, therefore, a part of its effect is included in the confining potential.

Chapter 3

Hamiltonian Set Up

3.1 Normal Mode Expansion and Choice of Potential

The bare parton fields have the following normal mode expansions (bare quark spinors u, v, helicity, $\lambda = \pm 1$, and color vectors $\hat{\epsilon}_{\mathcal{C}=1,2,3}$)

$$\Psi(\boldsymbol{x}) = \int \frac{d\boldsymbol{k}}{(2\pi)^3} \left[u_\lambda(\boldsymbol{k}) b_{\lambda\mathcal{C}}(\boldsymbol{k}) + v_\lambda(-\boldsymbol{k}) d^\dagger_{\lambda\mathcal{C}}(-\boldsymbol{k}) \right] e^{i\boldsymbol{k}\cdot\boldsymbol{x}} \hat{\epsilon}_{\mathcal{C}} \tag{3.1}$$

$$\mathbf{A}^a(\boldsymbol{x}) = \int \frac{d\boldsymbol{k}}{(2\pi)^3} \frac{1}{\sqrt{2k}} [\mathbf{a}^a(\boldsymbol{k}) + \mathbf{a}^{a\dagger}(-\boldsymbol{k})] e^{i\boldsymbol{k}\cdot\boldsymbol{x}} \tag{3.2}$$

$$\mathbf{E}^a_{tr}(\boldsymbol{x}) = i \int \frac{d\boldsymbol{k}}{(2\pi)^3} \sqrt{\frac{k}{2}} [\mathbf{a}^a(\boldsymbol{k}) - \mathbf{a}^{a\dagger}(-\boldsymbol{k})] e^{i\boldsymbol{k}\cdot\boldsymbol{x}}, \tag{3.3}$$

with the Coulomb gauge transverse condition, $\boldsymbol{k} \cdot \mathbf{a}^a(\boldsymbol{k}) = 0$. Here $b_{\lambda\mathcal{C}}(\boldsymbol{k})$, $d_{\lambda\mathcal{C}}(\boldsymbol{-k})$ and $a^a_\mu(\boldsymbol{k})$ ($\mu = 0, \pm 1$) are the bare quark, anti-quark and gluon Fock operators, the latter satisfying the transverse commutation relations,

$$[a^a_\mu(\boldsymbol{k}), a^{b\dagger}_{\mu'}(\boldsymbol{k'})] = (2\pi)^3 \delta_{ab} \delta^3(\boldsymbol{k} - \boldsymbol{k'}) D_{\mu\mu'}(\boldsymbol{k}) \ , \tag{3.4}$$

with

$$D_{\mu\mu'}(\boldsymbol{k}) = \delta_{\mu\mu'} - (-1)^{\mu}\frac{k_\mu k_{-\mu'}}{k^2} \ . \tag{3.5}$$

Confinement is described by a Cornell type potential which, as already mentioned, is known from lattice studies (15) to have the shape of the vacuum expectation value of the rigorous Coulomb kernel:

$$\begin{aligned} \hat{V}(r = |\boldsymbol{x} - \boldsymbol{y}|) &= \hat{V}_C(r) + \hat{V}_L(r) && (3.6)\\ \hat{V}_C(r) &= -\frac{\alpha_s}{r} && (3.7)\\ \hat{V}_L(r) &= \sigma r, && (3.8) \end{aligned}$$

where the string tension, $\sigma = 0.135$ GeV^2, and $\alpha_s = \frac{g^2}{4\pi} = 0.4$ have been previously determined. The Fourier transform of $\hat{V}$ is denoted by V and in momentum space these potentials take the form $V_L(|\boldsymbol{p}|) = -8\pi\sigma/p^4$, $V_C(|\boldsymbol{p}|) = -4\pi\alpha_s/p^2$.

The infrared divergency of the linear potential represents a potential problem; however, it is cancelled by the self-energy and interaction terms. But this cancellation occurs only when the color structure of the state in consideration is a color singlet, as previously noted using this same Coulomb gauge Hamiltonian (5) and also in Bethe-Salpeter applications to the $q\overline{q}$ problem (19). States with a different color configuration fail to cancel these Hamiltonian contributions, leaving the singularity to dominate the integral. Thus, color confinement is a consistent consequence of this Hamiltonian formulation.

For comparison and also to provide hadronic structure sensitivity to potential form, predictions using a confining potential (18) with a renormalization improved short-ranged behavior are also reported. This potential was utilized in a previous meson study (10) and has the momentum space representation

$$V(|\boldsymbol{p}|) = \begin{cases} -\frac{8.04}{p^2}\frac{\ln^{-0.62}(\frac{p^2}{m_g^2}+0.82)}{\ln^{0.8}(\frac{p^2}{m_g^2}+1.41)} & p > m_g \\ -\frac{12.25 m_g^{1.93}}{p^{3.93}} & p < m_g \end{cases} \ . \tag{3.9}$$

The parameter m_g sets the scale and is related to the string tension, σ, by $m_g \cong \sqrt{8\pi\sigma/12.25} \approx 600$ MeV.

3.2 Hamiltonian g^2 Corrections

Previous applications of the present model (5; 6; 7; 8; 9) used this Hamiltonian but set the QCD coupling, g, to zero. This truncation eliminated the quark-gluon interaction, $\mathbf{J}^a \cdot \mathbf{A}^a$, or "hyperfine" term, Eq. 2.18, and also the non-linear (non-abelian) component of the color magnetic fields, Eqs. 2.12 and 2.17. Now, both are included so that the non-confining part of the Hamiltonian is consistent to order g^2.

3.2.1 Hyperfine correction

Following (10), the Hamiltonian term H_{qg} containing the $\mathbf{J}^a \cdot \mathbf{A}^a$ operators is included using perturbation theory to second order in g. Then, integrating over the gluonic degrees of freedom yields an effective quark hyperfine interaction with a $\mathbf{J}^a \cdot \mathbf{J}^a$ form. This contribution is represented by the Feynman diagrams in Fig. 3.1.

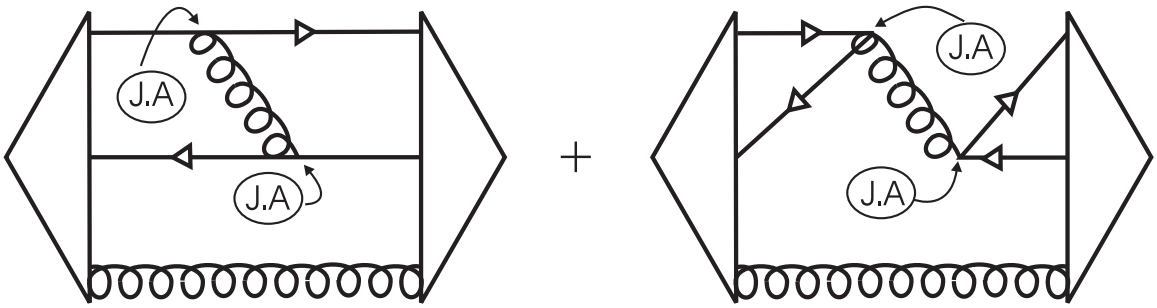

Figure 3.1: The hyperfine correction entails the exchange of a gluon between q and $\overline{q}$ and $q\overline{q}$ annihilation.

The resulting transverse hyperfine interaction is

$$V_T = \frac{1}{2}\iint d\boldsymbol{x} d\boldsymbol{y} J_i^a(\boldsymbol{x}) \hat{U}_{ij}(\boldsymbol{x},\boldsymbol{y}) J_j^a(\boldsymbol{y}), \tag{3.10}$$

where the kernel reflects the transverse gauge

$$\hat{U}_{ij}(\boldsymbol{x},\boldsymbol{y}) = \left(\delta_{ij} - \frac{\nabla_i \nabla_j}{\nabla^2}\right)_{\boldsymbol{x}} \hat{U}(|\boldsymbol{x}-\boldsymbol{y}|). \tag{3.11}$$

For $\hat{U}$ a modified Yukawa potential is chosen, which incorporates a dynamical mass, $m_g = 600$ MeV, for the exchanged gluon as explained in (10). Fourier transforming to momentum space, this continuous potential takes the form

$$U(p) = \begin{cases} -\frac{8.04}{p^2} \frac{\ln^{-0.62}(\frac{p^2}{m_g^2}+0.82)}{\ln^{0.8}(\frac{p^2}{m_g^2}+1.41)} & p > m_g \\ -\frac{24.50}{p^2+m_g^2} & p < m_g \end{cases} . \tag{3.12}$$

3.2.2 Non-abelian correction

Similarly, the non-abelian components of the color magnetic fields, $gf^{abc}\mathbf{A}^b \times \mathbf{A}^c$, in the kinetic energy are also included perturbatively through $(\mathbf{J}^a \cdot \mathbf{A}^a)(\mathbf{B}^a \cdot \mathbf{B}^a)$. The resulting non-abelian interaction is represented by the Feynman diagram in Fig. 3.2 and is given by

$$\begin{aligned} V_{NA} = \frac{1}{4}\iint d\boldsymbol{x} d\boldsymbol{y} f^{abc}\varepsilon_{ijk}\varepsilon_{ilm}[J_h^a(\boldsymbol{y})(\nabla_j^{(\boldsymbol{x})}\hat{U}_{kh}(\boldsymbol{x},\boldsymbol{y}))A_l^b(\boldsymbol{x})A_m^c(\boldsymbol{x}) + \\ J_h^b(\boldsymbol{y})(\nabla_j^{(\boldsymbol{x})}A_k^a(\boldsymbol{x}))\hat{U}_{lh}(\boldsymbol{x},\boldsymbol{y})A_m^c(\boldsymbol{x}) + J_h^c(\boldsymbol{y})(\nabla_j^{(\boldsymbol{x})}A_k^a(\boldsymbol{x}))A_l^b(\boldsymbol{x})\hat{U}_{mh}(\boldsymbol{x},\boldsymbol{y})], \end{aligned} \tag{3.13}$$

where $\hat{U}_{ij}$ is the same kernel appearing in the hyperfine potential.

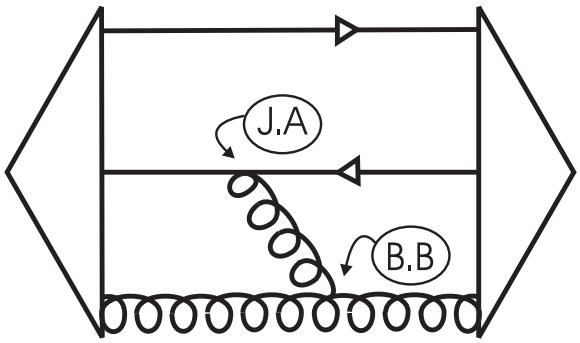

Figure 3.2: The non-abelian correction with triple gluon vertices.

Chapter 4

Gap Equations

Having defined the model Hamiltonian, the next step is to calculate the ground state. Since the field operators can be expanded in any complete basis, a BV rotation is performed,

$$\begin{aligned} B_{\lambda\mathcal{C}}(\boldsymbol{k}) &= \cos\frac{\theta_k}{2} b_{\lambda\mathcal{C}}(\boldsymbol{k}) - \lambda \sin\frac{\theta_k}{2} d^\dagger_{\lambda\mathcal{C}}(-\boldsymbol{k}) \\ D_{\lambda\mathcal{C}}(-\boldsymbol{k}) &= \cos\frac{\theta_k}{2} d_{\lambda\mathcal{C}}(-\boldsymbol{k}) + \lambda \sin\frac{\theta_k}{2} b^\dagger_{\lambda\mathcal{C}}(\boldsymbol{k}) \\ \boldsymbol{\alpha}^a(\boldsymbol{k}) &= \cosh\Theta_k \mathbf{a}^a(\boldsymbol{k}) + \sinh\Theta_k \mathbf{a}^{a\dagger}(-\boldsymbol{k}) \ , \end{aligned} \tag{4.1}$$

which transforms the bare particle operators $\mathbf{a}^a$, $b_{\lambda\mathcal{C}}$ and $d_{\lambda\mathcal{C}}$ into the dressed, quasi-particle operators $\boldsymbol{\alpha}^a$, $B_{\lambda\mathcal{C}}$ and $D_{\lambda\mathcal{C}}$, respectively. Now the fields are

$$\begin{aligned} \Psi(\boldsymbol{x}) &= \int \frac{d\boldsymbol{k}}{(2\pi)^3} \big[\mathcal{U}_\lambda(\boldsymbol{k}) B_{\lambda\mathcal{C}}(\boldsymbol{k}) + \mathcal{V}_\lambda(-\boldsymbol{k}) D^\dagger_{\lambda\mathcal{C}}(-\boldsymbol{k})\big] e^{i\boldsymbol{k}\cdot\boldsymbol{x}} \hat{\epsilon}_{\mathcal{C}} \\ \mathbf{A}^a(\boldsymbol{x}) &= \int \frac{d\boldsymbol{k}}{(2\pi)^3} \frac{1}{\sqrt{2\omega_k}} [\boldsymbol{\alpha}^a(\boldsymbol{k}) + \boldsymbol{\alpha}^{a\dagger}(-\boldsymbol{k})] e^{i\boldsymbol{k}\cdot\boldsymbol{x}} \\ \mathbf{E}^a_{tr}(\boldsymbol{x}) &= i \int \frac{d\boldsymbol{k}}{(2\pi)^3} \sqrt{\frac{\omega_k}{2}} [\boldsymbol{\alpha}^a(\boldsymbol{k}) - \boldsymbol{\alpha}^{a\dagger}(-\boldsymbol{k})] e^{i\boldsymbol{k}\cdot\boldsymbol{x}} \ , \end{aligned} \tag{4.2}$$

where $\omega_k = k e^{-2\Theta_k}$. Note that the dressed quark expansion remains functionally invariant with respect to the bare case since the quasi-particle spinors have the inverse

rotation

$$\begin{aligned}
\mathcal{U}_\lambda(\boldsymbol{k}) &= \cos\frac{\theta_k}{2}u_\lambda(\boldsymbol{k}) - \lambda\sin\frac{\theta_k}{2}v_\lambda(-\boldsymbol{k}) \\
&= \frac{1}{\sqrt{2}}\begin{bmatrix} \sqrt{1+\sin\phi_k}\ \ \chi_\lambda \\ \sqrt{1-\sin\phi_k}\ \boldsymbol{\sigma}\cdot\hat{\boldsymbol{k}}\ \ \chi_\lambda \end{bmatrix} \qquad (4.3) \\
\mathcal{V}_\lambda(-\boldsymbol{k}) &= \cos\frac{\theta_k}{2}v_\lambda(-\boldsymbol{k}) + \lambda\sin\frac{\theta_k}{2}u_\lambda(\boldsymbol{k}) \\
&= \frac{1}{\sqrt{2}}\begin{bmatrix} -\sqrt{1-\sin\phi_k}\ \boldsymbol{\sigma}\cdot\hat{\boldsymbol{k}}\ \ \chi_\lambda \\ \sqrt{1+\sin\phi_k}\ \ \chi_\lambda \end{bmatrix}. \qquad (4.4)
\end{aligned}$$

Here the quark gap angle, $\phi_k = \phi(k)$, is related to the BV angle θ_k by $\tan(\phi_k - \theta_k) = m/k$. The quasi-particle, BCS-like vacuum, defined by $B_{\lambda\mathcal{C}}|\Omega\rangle = D_{\lambda\mathcal{C}}|\Omega\rangle = \alpha^a_\mu|\Omega\rangle = 0$, is connected to the bare parton one, $b_{\lambda\mathcal{C}}|0\rangle = d_{\lambda\mathcal{C}}|0\rangle = a^a_\mu|0\rangle = 0$, by

$$|\Omega_{quark}\rangle = e^{-\int\frac{d\boldsymbol{k}}{(2\pi)^3}\lambda\tan\frac{\theta_k}{2}b^\dagger_{\lambda\mathcal{C}}(\boldsymbol{k})d^\dagger_{\lambda\mathcal{C}}(-\boldsymbol{k})}|0\rangle \qquad (4.5)$$

$$|\Omega_{gluon}\rangle = e^{-\int\frac{d\boldsymbol{k}}{(2\pi)^3}\frac{1}{2}\tanh\Theta_k D_{\mu\mu'}(\boldsymbol{k})a^{a\dagger}_\mu(\boldsymbol{k})a^{a\dagger}_{\mu'}(-\boldsymbol{k})}|0\rangle\ . \qquad (4.6)$$

The ground state, $|\Omega\rangle = |\Omega_{quark}\rangle\otimes|\Omega_{gluon}\rangle$, now contains quark and gluon condensates (correlated $q\bar{q}$ and gg Cooper pairs). Performing a variational minimization of the vacuum expectation value of the Hamiltonian, $\delta\langle\Omega|H_{\rm eff}|\Omega\rangle = 0$, independently with respect to ϕ_k and ω_k, yields the mass gap equations for each sector

$$\begin{aligned}
ks_k - mc_k &= \frac{2}{3}\int\frac{d\boldsymbol{q}}{(2\pi)^3}\left[(s_kc_qx - s_qc_k)V(|\boldsymbol{k}-\boldsymbol{q}|)\right. \\
&- \left. 2c_ks_qU(|\boldsymbol{k}-\boldsymbol{q}|) + 2c_qs_kW(|\boldsymbol{k}-\boldsymbol{q}|)\right] \qquad (4.7)
\end{aligned}$$

$$\begin{aligned}
\omega_k^2 &= k^2 - \frac{3}{4}\int\frac{d\boldsymbol{q}}{(2\pi)^3}V(|\boldsymbol{k}-\boldsymbol{q}|)[1+x^2]\left(\frac{\omega_q^2-\omega_k^2}{\omega_q}\right) \\
&+ \frac{3}{4}\,g^2\int\frac{d\boldsymbol{q}}{(2\pi)^3}\frac{1-x^2}{\omega_q}\ , \qquad (4.8)
\end{aligned}$$

where

$$W(|\boldsymbol{k}-\boldsymbol{q}|) \equiv U(|\boldsymbol{k}-\boldsymbol{q}|)\frac{x(k^2+q^2)-qk(1+x^2)}{|\boldsymbol{k}-\boldsymbol{q}|^2}\ , \tag{4.9}$$

with $s_k = \sin\phi_k$, $c_k = \cos\phi_k$ and $x = \boldsymbol{k}\cdot\boldsymbol{q}$. The last term in Eq. (4.8) originates from the non-abelian component of the gluon kinetic energy. Dimensional analysis of the above integrals reveals that the first equation is UV finite for the linear potential since $V_L(|\boldsymbol{p}|) = -8\pi\sigma/p^4$, but not for the Coulomb potential $V_C(|\boldsymbol{p}|) = -4\pi\alpha_s/p^2$. In Eq. (4.8) there are both logarithmical and quadratical divergences in the UV region and an integration cutoff, $\Lambda = 4$ GeV, determined in previous studies is used.

Once the current quark masses are fixed, the gap equations can be solved numerically for the quark and gluon gap angles and, then, the quark-antiquark and the gluon condensates can be calculated,

$$\langle\overline{q}q\rangle \equiv \langle\Omega|\overline{\Psi}(0)\Psi(0)|\Omega\rangle = -\frac{3}{\pi^2}\int k^2\left(s_k - \frac{m}{E_k}\right)dk, \tag{4.10}$$

$$\langle gg\rangle \equiv \langle\Omega|\frac{\alpha_s}{\pi}F_a^{\mu\nu}F^a_{\mu\nu}|\Omega\rangle = \frac{4}{\pi^2}\int q^2\left(\frac{\omega_q^2+q^2-2qw_q}{w_q}\right)dq, \tag{4.11}$$

respectively. Here, the trivial ($\theta = 0$) quark condensate contribution has been subtracted to regulate the otherwise divergent integrals (unless the quark mass is zero), and only the abelian part of $F^a_{\mu\nu}$ has been taken (i.e., up to order g^0). Using $m_u = m_d = 5MeV$ for the u and d quarks, the quark condensate is $\langle\overline{q}q\rangle = (-127\,MeV)^3$, smaller than the lattice result, $(-270\,MeV)^3$, suggesting an improved ground state, including more correlations, is needed. In the gluon case, the condensate value is $\langle gg\rangle = (433\,MeV)^4$, in good agreement with the QCD sum rule result, $(441\,MeV)^4$.

Using $|q\rangle = B_{\lambda\mathcal{C}}(\boldsymbol{k})^\dagger|\Omega\rangle$ and $|g\rangle = \alpha^a_\mu(\boldsymbol{k})^\dagger|\Omega\rangle$, the quark and gluon self-energies are respectively

$$\epsilon_k \equiv \langle q|H_{\rm eff}|q\rangle = ms_k + kc_k - \tag{4.12}$$
$$\frac{2}{3}\int\frac{d\boldsymbol{q}}{(2\pi)^3}\left[(s_k s_q + c_q c_k x)V(|\boldsymbol{k}-\boldsymbol{q}|) + 2s_k s_q U(|\boldsymbol{k}-\boldsymbol{q}|) + 2c_q c_k W(|\boldsymbol{k}-\boldsymbol{q}|)\right]$$

and, for fixed color index a (no sum),

$$\begin{aligned}\varepsilon_k^{\mu\mu'} &\equiv \langle\Omega|\alpha_\mu^a(\boldsymbol{k})\, H_{\rm eff}\, \alpha_{\mu'}^a(\boldsymbol{k})^\dagger|\Omega\rangle \\ &= \frac{\omega_k^2+k^2}{2\omega_k}\delta_{\mu\mu'} - \frac{3}{4}\int\frac{d\boldsymbol{q}}{(2\pi)^3}V(|\boldsymbol{k}-\boldsymbol{q}|)\frac{\omega_k^2+\omega_q^2}{\omega_q\omega_k}D_{\mu\mu'}(\boldsymbol{q}) \\ &+ \frac{9}{2}g^2\int\frac{d\boldsymbol{q}}{(2\pi)^3}\frac{1}{2\omega_k\omega_q}\times\left[2D_{\mu\mu'}(\boldsymbol{k}) - D_{\mu\nu}(\boldsymbol{k})D_{\nu\nu'}(\boldsymbol{q})D_{\nu'\mu'}(\boldsymbol{k})\right]\ ,\end{aligned} \tag{4.13}$$

both of which are infrared divergent in the presence of an infrared enhanced kernel. This is a welcomed feature of this approach, as colored states are removed from the spectrum, as required by confinement. The infrared divergence cancels, however, for color singlet states in bound state equations, leading to a physical spectrum of mesons and baryons.

Even though the self-energy is divergent, following the prescriptions from (19) a quark (quasi-particle) running mass, $M_q(k)$, can still be defined. Its value at $k=0$ gives the constituent mass, M_q, whose value can be extracted from the low momentum behavior of the gap angle, by introducing a canonical Dirac spinor,

$$U_\lambda(\boldsymbol{k}) = N\begin{pmatrix}\chi_\lambda \\ \frac{\boldsymbol{\sigma}\cdot\boldsymbol{k}}{E+M_q(\boldsymbol{k})}\chi_\lambda\end{pmatrix}, \tag{4.14}$$

with normalization N and $E=\sqrt{M_q^2(\boldsymbol{k})+k^2}$, which when compared to eq. (4.3) yields the relation

$$\frac{\sqrt{1+\sin\phi_k}}{\sqrt{1-\sin\phi_k}} = \frac{E+M_q(\boldsymbol{k})}{k} \Longrightarrow \sin\phi_k = \frac{M_q(\boldsymbol{k})}{\sqrt{M_q^2(\boldsymbol{k})+k^2}}. \tag{4.15}$$

Expanding last equation around $k = 0$, the defining relation for the running mass, $M_q(\boldsymbol{k})$, is obtained

$$\sin\phi_k \simeq 1 - \frac{k^2}{2M_q^2(\boldsymbol{k})}. \tag{4.16}$$

A similar argument can be drawn for the gluon case. Figure 4.1 details the quasi-particle (running) energies for the u/d, s and c quarks and the gluon.

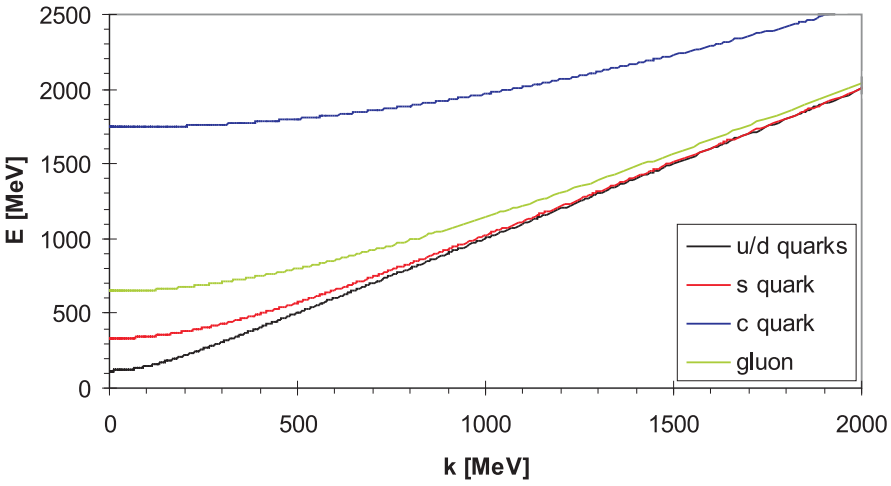

Figure 4.1: Quasi-particle energies for the u/d, s and c quarks and for the gluon ($E(k) = \sqrt{k^2 + M_q(k)^2}$ for quarks and $\omega(k)$ for gluons).

In summary, the BV/BCS procedure described above helps to understand the physics of the problem. The ground state that minimizes the total energy does not have the symmetries of the original Hamiltonian, hence, a BV rotation has to be performed in order to pick a convenient basis. A BCS-like ansatz for the ground state, eqs. (4.5) and (4.6), explicitly expresses its Cooper pair structure, responsible for breaking the Hamiltonian's chiral symmetry and generating masses for quarks and gluons. Finally, the procedure leads to a gap equation for each sector, representing the conditions for minimizing the total energy.

Chapter 5

Hybrid Mesons

Following the "Eightfold Way" (Gell-Mann and Ne'eman), the "Quark Model" (Gell-Mann and Zweig), along with subsequent extensions, has generally explained the observed hadronic spectrum. This is especially true for heavy flavored mesons where it is now clear that higher order QCD corrections can be ignored or treated perturbatively. Even in the light sector, the phenomenological quark model works reasonably well. However, the existence of hadrons with exotic quantum numbers (i.e. J^{PC} states not possible in $q\bar{q}$ or qqq systems) clearly reveals this model is not complete. Related, it is expected that there are exotic hadrons with conventional quantum numbers that also can not be described by the quark model, e.g., glueballs gg, hybrid mesons $q\bar{q}g$ and tetraquarks $q\bar{q}q\bar{q}$.

Possible experimental evidence for a 1^{-+} exotic state was first reported in 1988 (20), but the situation was not clarified until several years later. Now it is believed that there exist two states with these quantum numbers below 2 GeV: $\pi_1(1400)$ (21; 22) and $\pi_1(1600)$ (23; 24)(note, a recent analysis (25) finds no evidence for either candidate). There are also other reported hybrid candidates with $J^{PC} = 0^{-+}$ (26; 27), 1^{--} (28) and 2^{-+} (29; 30; 31).

Theoretically, the structure of the π_1 states remains unclear. They could be hybrid or tetraquark mesons with most theoretical studies (32; 33) investigating the former.

Table 5.1: Predicted 1^{-+} masses, in GeV, for light, strange and charmed hybrid mesons.

Model [Reference]	u/d hybrid	s hybrid	c hybrid
QCD (34; 35; 36; 37; 38; 44; 45; 46)	1.7 - 2.1	1.9	4.2 - 4.4
Flux Tube (39; 40; 41)	1.8 - 2.1	2.1 - 2.3	4.1 - 4.5
Bag Model (42)	1.3 - 1.8		3.9

Lattice gauge simulations (34; 35; 36; 37; 38) predict the lightest hybrid meson is between 1.7 and 2.1 GeV and results from the Flux Tube model (39; 40; 41) also span much of this range. Only vintage Bag model (42) calculations yield a lower mass, between 1.3 and 1.8 GeV, but Ref. (43) argues that the $\pi_1(1400)$ is not a hybrid. Table 5.1 lists predictions for the u/d, s and c 1^{-+} hybrid mesons.

The framework developed above is now applied to resolve this important problem. This extends an earlier hybrid calculation (7) by including previously omitted terms in the Hamiltonian and by comprehensively predicting the light, strange and charmed hybrid meson spectra.

5.1 Construction of hybrid mesons

5.1.1 Wavefunction ansatz and quantum numbers

Following an initial study (7), the hybrid center of momentum system is chosen as the reference frame and the momenta of the dressed quark, anti-quark and gluon are denoted by $\boldsymbol{q}$, $\bar{\boldsymbol{q}}$ and $\boldsymbol{g}$, respectively. Next, define $\boldsymbol{q}_+ \equiv \frac{\boldsymbol{q}+\overline{\boldsymbol{q}}}{2}$, $\boldsymbol{q}_- \equiv \boldsymbol{q} - \overline{\boldsymbol{q}}$ and note that $\boldsymbol{g} = -\boldsymbol{q} - \overline{\boldsymbol{q}} = -2\boldsymbol{q}_+$.

The color structure of a $q\bar{q}g$ hybrid is determined by SU(3) algebra

$$\begin{aligned}(3 \otimes \overline{3}) \otimes 8 &= (8 \oplus 1) \otimes 8 = (8 \otimes 8) \oplus (8 \otimes 1) \\ &= 27 \oplus 10 \oplus 10 \oplus 8 \oplus 8 \oplus 1 \oplus 8. \end{aligned} \tag{5.1}$$

Note for an overall color singlet the quarks must be in an octet state like the gluon.

As discussed below, this leads to a repulsive $q\bar{q}$ interaction, confirmed by lattice at short range, which raises the mass of the hybrid meson. The hybrid wavefunction will therefore involve the color structure $T^a_{\mathcal{C}_1\mathcal{C}_2}B^\dagger_{\mathcal{C}_1}D^\dagger_{\mathcal{C}_2}\alpha^{a\dagger}$ and has the general form

$$|\Psi^{JPC}\rangle = \iint \frac{d\boldsymbol{q}_+ d\boldsymbol{q}_-}{(2\pi)^6}\,\Phi^{JPC}_{\lambda_1\lambda_2\mu}(\boldsymbol{q}_+,\boldsymbol{q}_-)T^a_{\mathcal{C}_1\mathcal{C}_2}B^\dagger_{\lambda_1\mathcal{C}_1}(\boldsymbol{q})D^\dagger_{\lambda_2\mathcal{C}_2}(\overline{\boldsymbol{q}})\alpha^{a\dagger}_\mu(\boldsymbol{g})|\Omega\rangle\ , \tag{5.2}$$

which is summed over color and angular momentum magnetic sub-states.

There are five angular momenta in this system, two orbital, $\mathbf{l}_\pm$ (associated with $\boldsymbol{q}_\pm$) having z projections $m_\pm$, and the 3 spins, $S_q = S_{\overline{q}} = 1/2$ and $S_g = 1$ with projections λ_1, λ_2 and μ, respectively. To form states with total angular momentum J, projection m_J, the following coupling scheme is used, $\boldsymbol{S} = \boldsymbol{S}_q + \boldsymbol{S}_{\overline{q}}$, $\boldsymbol{j} = \boldsymbol{S}_g + \boldsymbol{l}_+$, $\boldsymbol{L} = \boldsymbol{j} + \boldsymbol{l}_-$, $\boldsymbol{J} = \boldsymbol{L} + \boldsymbol{S}$. Then with the appropriate Clebsch-Gordan coefficients, the hybrid wavefunction can be expressed in terms of a radial wavefunction $F^{JPC}(q_+, q_-)$ and spherical harmonics, $Y^{m_\pm}_{l_\pm}(\boldsymbol{q}_\pm)$,

$$\begin{aligned}\Phi^{JPC}_{\lambda_1\lambda_2\mu}(\boldsymbol{q}_+,\boldsymbol{q}_-) = F^{JPC}(q_+,q_-)Y^{m_+}_{l_+}(\hat{\boldsymbol{q}}_+)Y^{m_-}_{l_-}(\hat{\boldsymbol{q}}_-)(-1)^{\frac{1}{2}-\lambda_2}\langle\tfrac{1}{2}\tfrac{1}{2},\lambda_1(-\lambda_2)|Sm_S\rangle \\ (-1)^\mu\langle 1l_+,(-\mu)m_+|jm_j\rangle\langle jl_-,m_jm_-|Lm_L\rangle\langle LS,m_Lm_S|JM_J\rangle.\end{aligned} \tag{5.3}$$

Since the intrinsic parity for a $q\bar{q}$ pair and a gluon are both -1, and the two orbital parities are $(-1)^{l_-}$ and $(-1)^{l_+}$, the total hybrid meson parity is

$$P = (-1)(-1)(-1)^{l_+}(-1)^{l_-} = (-1)^{l_+ + l_-}. \tag{5.4}$$

Finally, exchanging all additive quantum numbers, as required by charge conjugation, yields a $(-1)^{l_- + S}$ factor from the space and spinor $q\overline{q}$ components which needs to be combined with the phase of the $q\overline{q}g$ composite color component. Although the gluon octet is not an eigenstate of C-parity, each gluon has a $q\overline{q}$ octet partner with opposite C-parity, resulting in a -1 contribution for the combined $[[3\otimes\bar{3}]_8\otimes 8]_1$

Table 5.2: Hybrid meson quantum numbers up to $J = 3$. Note exotic states and states forbidden by transversality: $l_+ = 1$ cannot couple to $j = 0$.

l_+	l_-	S	j	L	J	P	C	J^{PC}	
0	0	0	1	1	1	+	-	1^{+-}	
0	0	1	1	1	0	+	+	0^{++}	
0	0	1	1	1	1	+	+	1^{++}	
0	0	1	1	1	2	+	+	2^{++}	
0	1	0	1	0	0	-	+	0^{-+}	
0	1	0	1	1	1	-	+	1^{-+}	Exotic
0	1	0	1	2	2	-	+	2^{-+}	
0	1	1	1	0	1	-	-	1^{--}	
0	1	1	1	1	0	-	-	0^{--}	Exotic
0	1	1	1	1	1	-	-	1^{--}	
0	1	1	1	1	2	-	-	2^{--}	
0	1	1	1	2	1	-	-	1^{--}	
0	1	1	1	2	2	-	-	2^{--}	
0	1	1	1	2	3	-	-	3^{--}	
1	0	0	0	0	0	-	-	0^{--}	Forbidden
1	0	0	1	1	1	-	-	1^{--}	
1	0	0	2	2	2	-	-	2^{--}	
1	0	1	0	0	1	-	+	1^{-+}	Forbidden
1	0	1	1	1	0	-	+	0^{-+}	
1	0	1	1	1	1	-	+	1^{-+}	Exotic
1	0	1	1	1	2	-	+	2^{-+}	
1	0	1	2	2	1	-	+	1^{-+}	Exotic
1	0	1	2	2	2	-	+	2^{-+}	
1	0	1	2	2	3	-	+	3^{-+}	Exotic

system. Therefore the hybrid C-parity is

$$C = (-1)(-1)^{l_- + S} = (-1)^{1 + l_- + S}. \tag{5.5}$$

The extra -1 phase, as compared to a conventional $q\overline{q}$ meson having C-parity $(-1)^{l_- + S}$, is responsible for generating exotic quantum numbers for certain hybrid states (e.g. $J^{PC} = 1^{-+}$). Table 5.2 lists quantum numbers for the model hybrid states for J up to 3. Note the exotic quantum number states and also states forbidden by the Coulomb gauge transversality condition (gluon orbital $l_+ = 1$ can not couple with its spin to produce $j = 0$).

5.1.2 Variational equations of motion

The hybrid mass, M_{JPC}, is now computed for each J^{PC} with special interest focusing upon the exotic states. In terms of the above variational wavefunction, an upper bound for the mass is given by

$$\begin{aligned} M_{JPC} &= \frac{\langle \Psi^{JPC} | H_{\rm eff} | \Psi^{JPC} \rangle}{\langle \Psi^{JPC} | \Psi^{JPC} \rangle} \\ &= M_{self} + M_{q\overline{q}} + M_{qg} + M_{qgq} + M_{ggg} \ . \end{aligned} \tag{5.6}$$

Here, the subscripts indicate the mass contribution from the self-energy of the three constituents, M_{self}, the $q\overline{q}$ interaction, $M_{q\overline{q}}$, the qg and $\overline{q}g$ interactions, M_{qg}, the 2^{nd} order correction from the qgq and $\overline{q}g\overline{q}$ vertices, M_{qgq}, and the 2^{nd} order correction from triple gluon vertices, M_{ggg}. The three-body expectation value entails twelve dimensional integrals which can be reduced to nine dimensions by working in the center of momentum. The detailed expressions are

$$M_{\rm self} = \iint \frac{d\boldsymbol{q}\, d\overline{\boldsymbol{q}}}{(2\pi)^6} \Phi^{JPC\dagger}_{\lambda_1\lambda_2\mu}(\boldsymbol{q}, \overline{\boldsymbol{q}}) \Phi^{JPC}_{\lambda_1\lambda_2\mu'}(\boldsymbol{q}, \overline{\boldsymbol{q}}) \left[D_{\nu\nu'}(\boldsymbol{g})(\epsilon_{\boldsymbol{q}} + \epsilon_{\overline{\boldsymbol{q}}}) + D_{\mu\nu}(\boldsymbol{g}) D_{\mu'\nu'}(\boldsymbol{g}) \varepsilon^{\nu\nu'}_{\boldsymbol{g}} \right] \tag{5.7}$$

$$M_{q\overline{q}} = -\frac{1}{2}\iiint \frac{d\boldsymbol{q}\, d\overline{\boldsymbol{q}}\, d\boldsymbol{q'}}{(2\pi)^9}\Phi^{JPC\dagger}_{\lambda_1\lambda_2\mu}(\boldsymbol{q},\overline{\boldsymbol{q}})\Phi^{JPC}_{\lambda_1'\lambda_2'\mu'}(\boldsymbol{q'},\boldsymbol{q}+\overline{\boldsymbol{q}}-\boldsymbol{q'})D_{\mu\mu'}(\boldsymbol{g}) \tag{5.8}$$
$$\left[\frac{1}{3}V(|\boldsymbol{q'}-\boldsymbol{q}|)\mathcal{U}^\dagger_{\lambda_1\boldsymbol{q}}\mathcal{U}_{\lambda_1'\boldsymbol{q'}}\mathcal{V}^\dagger_{\lambda_2'\boldsymbol{q}+\overline{\boldsymbol{q}}-\boldsymbol{q'}}\mathcal{V}_{\lambda_2\overline{\boldsymbol{q}}} + V(|\boldsymbol{q}+\overline{\boldsymbol{q}}|)\mathcal{U}^\dagger_{\lambda_1\boldsymbol{q}}\mathcal{V}_{\lambda_2\overline{\boldsymbol{q}}}\mathcal{V}^\dagger_{\lambda_2'\boldsymbol{q}+\overline{\boldsymbol{q}}-\boldsymbol{q'}}\mathcal{U}_{\lambda_1'\boldsymbol{q'}}\right]$$

$$M_{qg} = \frac{3}{4}\iiint \frac{d\boldsymbol{q}\, d\overline{\boldsymbol{q}}\, d\boldsymbol{q'}}{(2\pi)^9}\Phi^{JPC\dagger}_{\lambda_1\lambda_2\mu}(\boldsymbol{q},\overline{\boldsymbol{q}}) \tag{5.9}$$
$$\left[\frac{\omega_{q+\overline{q}}+\omega_{q'+\overline{q}}}{\sqrt{\omega_{q+\overline{q}}\ \omega_{q'+\overline{q}}}}\Phi^{JPC}_{\lambda\lambda_2\mu'}(\boldsymbol{q'},\overline{\boldsymbol{q}})D_{\mu'\mu''}(\boldsymbol{q}+\overline{\boldsymbol{q}})D_{\mu\mu''}(\boldsymbol{q}+\overline{\boldsymbol{q}})V(|\boldsymbol{q}-\boldsymbol{q'}|)\mathcal{U}^\dagger_{\lambda\boldsymbol{q'}}\mathcal{U}_{\lambda_1\boldsymbol{q}} +\right.$$
$$\left.\frac{\omega_{q+\overline{q}}+\omega_{q+q'}}{\sqrt{\omega_{q+\overline{q}}\ \omega_{q+q'}}}\Phi^{JPC}_{\lambda_1\lambda\mu'}(\boldsymbol{q},\boldsymbol{q'})D_{\mu'\mu''}(\boldsymbol{q}+\boldsymbol{q'})D_{\mu''\mu}(\boldsymbol{q}+\overline{\boldsymbol{q}})V(|\overline{\boldsymbol{q}}-\boldsymbol{q'}|)\mathcal{V}^\dagger_{\lambda\boldsymbol{q'}}\mathcal{V}_{\lambda_2\overline{\boldsymbol{q}}}\right]$$

$$M_{qgq} = \frac{1}{2}\iiint \frac{d\boldsymbol{q}\, d\overline{\boldsymbol{q}}\, d\boldsymbol{q'}}{(2\pi)^9}\Phi^{JPC\dagger}_{\lambda_1\lambda_2\mu}(\boldsymbol{q},\overline{\boldsymbol{q}})\Phi^{JPC}_{\lambda_1'\lambda_2'\mu'}(\boldsymbol{q'},\boldsymbol{q}+\overline{\boldsymbol{q}}-\boldsymbol{q'})D_{\mu\mu'}(\boldsymbol{g})\mathcal{U}^\dagger_{\lambda_1\boldsymbol{q}} \tag{5.10}$$
$$\left[\frac{1}{3}U_{mn}(\boldsymbol{q'}-\boldsymbol{q})\alpha_m\mathcal{U}_{\lambda_1'\boldsymbol{q'}}\mathcal{V}^\dagger_{\lambda_2'\boldsymbol{q}+\overline{\boldsymbol{q}}-\boldsymbol{q'}}\alpha_n\mathcal{V}_{\lambda_2\overline{\boldsymbol{q}}} + U_{mn}(\boldsymbol{q}+\overline{\boldsymbol{q}})\alpha_m\mathcal{V}_{\lambda_2\overline{\boldsymbol{q}}}\mathcal{V}^\dagger_{\lambda_2'\boldsymbol{q}+\overline{\boldsymbol{q}}-\boldsymbol{q'}}\alpha_n\mathcal{U}_{\lambda_1'\boldsymbol{q'}}\right]$$

$$M_{ggg} = \frac{3}{8}i\iiint \frac{d\boldsymbol{q}\, d\overline{\boldsymbol{q}}\, d\boldsymbol{q'}}{(2\pi)^9}\frac{\Phi^{JPC\dagger}_{\lambda_1\lambda_2\mu}(\boldsymbol{q},\overline{\boldsymbol{q}})\Phi^{JPC}_{\lambda_1'\lambda_2\mu'}(\boldsymbol{q'},\overline{\boldsymbol{q}})}{\sqrt{\omega_{-q'-\overline{q}}\,\omega_{q+\overline{q}}}}(\mathcal{U}^\dagger_{\lambda_1\boldsymbol{q}}\alpha_h\mathcal{U}_{\lambda_1'\boldsymbol{q'}} + \mathcal{V}^\dagger_{\lambda_1\boldsymbol{q}}\alpha_h\mathcal{V}_{\lambda_1'\boldsymbol{q'}}) \tag{5.11}$$
$$\Big\{\nabla_l U_{kh}(\boldsymbol{q}-\boldsymbol{q'})\Big[D_{\mu k}(\boldsymbol{g})D_{l\mu'}(-\boldsymbol{q'}-\overline{\boldsymbol{q}}) - D_{\mu l}(\boldsymbol{g})D_{k\mu'}(-\boldsymbol{q'}-\overline{\boldsymbol{q}})\Big]$$
$$+i(\boldsymbol{q}-\boldsymbol{q'})_l U_{lh}(\boldsymbol{q'}+\boldsymbol{q})D_{\mu k}(\boldsymbol{g})D_{k\mu'}(-\boldsymbol{q'}-\overline{\boldsymbol{q}})$$
$$-iU_{kh}(\boldsymbol{q}-\boldsymbol{q'})\Big[(\boldsymbol{q'}+\overline{\boldsymbol{q}})_l D_{\mu l}(\boldsymbol{g})D_{k\mu'}(-\boldsymbol{q'}-\overline{\boldsymbol{q}}) + (\boldsymbol{q}+\overline{\boldsymbol{q}})_l D_{\mu k}(\boldsymbol{g})D_{l\mu'}(-\boldsymbol{q'}-\overline{\boldsymbol{q}})\Big]\Big\}.$$

Here, $\epsilon_{\boldsymbol{q}}$, $\epsilon_{\overline{\boldsymbol{q}}}$ and $\varepsilon^{\mu\mu'}_{\boldsymbol{g}}$ are the quark, anti-quark and gluon self-energies, respectively, evaluated at the indicated momentum ($\boldsymbol{g} = -\boldsymbol{q} - \overline{\boldsymbol{q}}$). A pictorial representation for

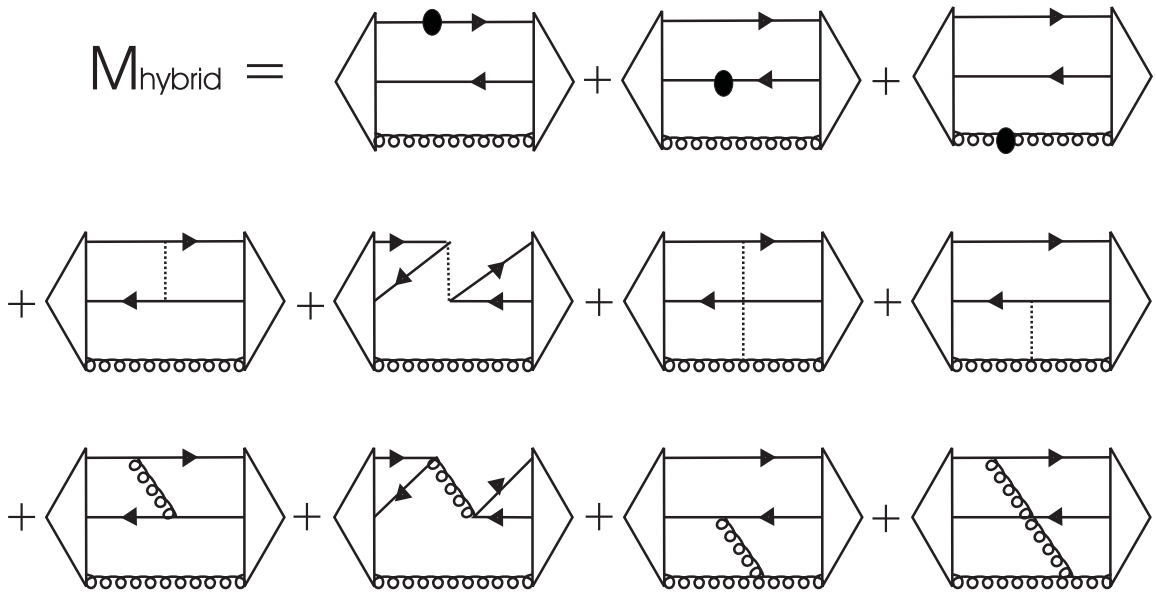

Figure 5.1: Diagrams for $\langle \Psi^{JPC} | H_{\rm eff} | \Psi^{JPC} \rangle$.

each type of contribution is given by the Feynman diagrams in Fig. 5.1.

The above expectation values are then computed variationally using the separable radial wavefunction, $F(q_+, q_-) = f(q_+, \alpha_+) f(q_-, \alpha_-)$, having two variational parameters, α_+ and α_-. Two functional forms for f were investigated; a gaussian and a scalable, numerical solution from previous two body meson studies. In general, the gaussian radial wavefunction,

$$f(q_\pm, \alpha_\pm) = e^{-x_\pm^2}, \quad x_\pm = \frac{q_\pm}{\alpha_\pm} \tag{5.12}$$

provided better results (lower variational mass) for s-wave states when compared to the numerical one. This was also true for p-wave orbital excitations, provided the gaussian was multiplied by $x_\pm$ corresponding to $l_\pm = 1$.

All integrals were calculated using the Monte Carlo method with the adaptive sampling algorithm VEGAS (47). This algorithm is based on importance sampling; it samples the integrand, so that the Monte-Carlo points are concentrated in the regions that make the largest contribution to the integral. In the fortran code developed to

solve equation (5.6), the VEGAS subroutine is called several times ($\simeq 7$) with an increasing number of points, from 64,000 up to 4,096,000 (doubling the number each time), until a weight-averaged result converges. The hybrid mass error introduced by this procedure is about ± 50 MeV.

For each J^{PC} hybrid state the variational parameters, α_+ and α_-, were optimized to produce the lowest mass. In terms of the string tension, their values fell in the ranges $0.9\sqrt{\sigma} \leq \alpha_+ \leq 1.7\sqrt{\sigma}$ and $1.0\sqrt{\sigma} \leq \alpha_- \leq 3.3\sqrt{\sigma}$. For an example of the energy surface generated when varying the parameters, see Fig. 5.2.

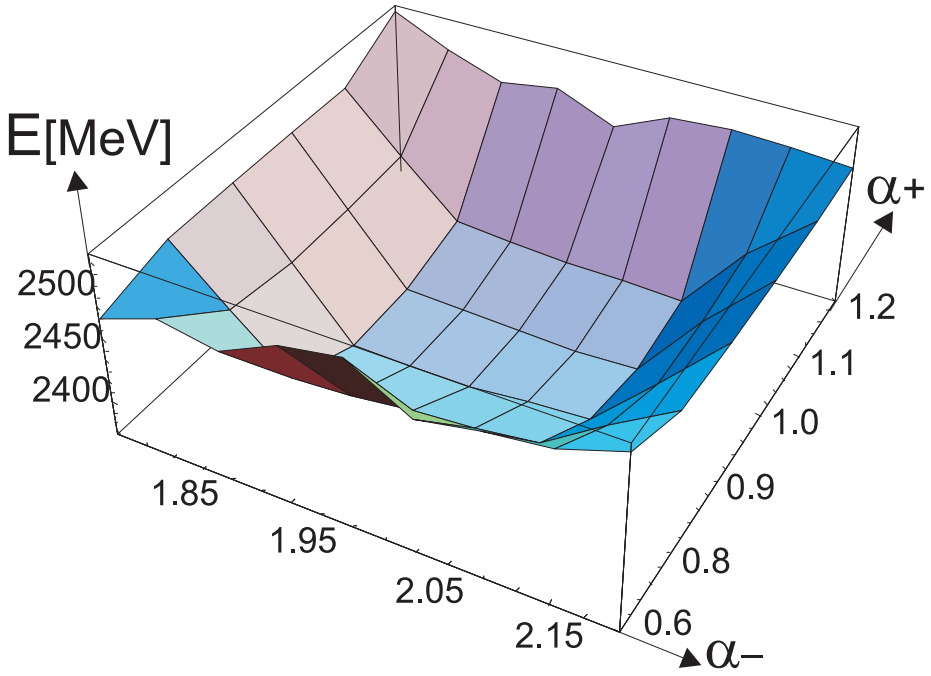

Figure 5.2: Energy surface of a 1^{-+} state as a function of the variational parameters

5.2 Results: Hybrid Meson Spectrum

5.2.1 Light hybrid mesons

For the light hybrid calculation, $m = 5$ MeV (48) was used for the u/d current quark mass. Results are listed in Table 5.3 which shows the ground state is the 0^{++} non-exotic scalar, followed by the triplet 1^{+-}, 2^{++} and 1^{++}. The lightest hybrid mass is 2.1 GeV.

Table 5.3: Spectrum of light hybrid meson states. Error $\approx \pm$ 50 MeV. *Isospin degenerate states.

$(I)J^{PC}$	M_{JPC} (MeV) no corrections	M_{JPC} (MeV) with g^2 corrections	
$(0)0^{++}$	2080	2135	
$(1)0^{++}$	2065	2100	Ground
$(0)1^{+-}$	2135	2140	*
$(1)1^{+-}$	2135	2140	*
$(0)2^{++}$	2340	2335	
$(1)2^{++}$	2180	2170	
$(0)1^{++}$	2415	2470	
$(1)1^{++}$	2110	2170	
$(0)1^{-+}$	2500	2525	Exotic
$(1)1^{-+}$	2205	2220	Exotic
$(0)0^{--}$	2275	2280	Exotic
$(1)0^{--}$	2280	2285	Exotic
$(0)1^{-+}$	2370	2400	Exotic *
$(1)1^{-+}$	2370	2400	Exotic *
$(0)1^{-+}$	2760	2790	Exotic
$(1)1^{-+}$	2570	2600	Exotic
$(0)3^{-+}$	3030	3040	Exotic
$(1)3^{-+}$	2910	2915	Exotic

For exotic states, as can be seen from Table 5.2, at least one p-wave in $\boldsymbol{q}_+$ or $\boldsymbol{q}_-$ is required. Because the $q\bar{q}$ interaction is repulsive for quarks in a color octet state, the excitation energy is less for a l_+ (gluon orbital) excitation than a l_- ($q\bar{q}$ orbital) excitation since the quarks are further separated and experience a larger repulsive

linear force.

The lightest exotic state is the $I = 1, 1^{-+}$, with mass 2.22 GeV. This is slightly higher than the Flux Tube model and lattice QCD predicted masses for this state, which were between 1.7 and 2.1 GeV (see Table 5.1).

The effects of including the non-abelian (NA) and hyperfine corrections were studied for several states. Generally, both effects were small (except the hyperfine correction for charmed quarks, see below), roughly of the same order as the overall 50 MeV Monte Carlo error. In particular, the NA correction entailed several terms with different signs which tended to cancel.

The model exotic spectrum (see Fig. 5.3) spans almost a GeV, between 2.1 and about 3 GeV, and includes predictions for J up to 3. There are no exotic $J = 2$ model states in this region since they require a d-wave or two p-waves, both involving much higher excitations.

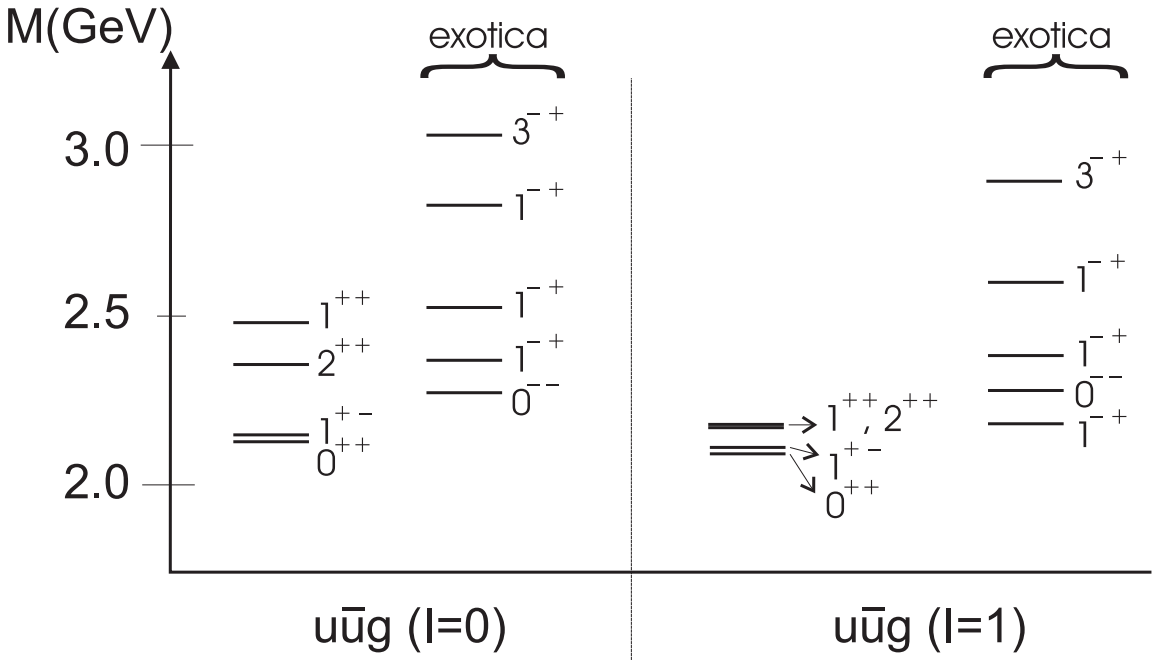

Figure 5.3: $u\bar{u}g$ spectrum.

Finally, note an interesting isospin splitting effect. From Fig. 5.1, annihilation

terms only contribute to the hybrid mass if the $q\overline{q}$ pair has quantum numbers consistent with the interaction. This is satisfied when $I_{q\overline{q}} = 0$ and $S = 1$. The annihilation diagrams can increase the $I = 0$ hybrid states by several hundred MeV, as detailed in Table 5.3. In other cases, the 1^{+-} and one of the 1^{-+} states should be isospin degenerate, as is computed to within the Monte Carlo error. On the other hand, the states 0^{++} and 0^{--} are not expected to be degenerate but, within the error, they are. It may be that the isospin splitting is not zero, but rather is smaller than the numerical error. Note the annihilation process for s-wave, isoscalar quarks in a triplet spin state is analogous to e^-e^+ annihilation in the triplet state of positronium.

5.2.2 Strange hybrid mesons

Table 5.4 summarizes results obtained for the $s\bar{s}g$ (hidden strangeness) hybrid mesons using a bare strange quark mass of 80 MeV. Now, the ground state is given by the non-exotic pseudovector state 1^{+-}, with a 2.125 GeV mass, not at all reflecting the 75 MeV additional quark flavor mass contribution (the hybrid calculation is only sensitive to current quark masses above 200 MeV). This prediction is in good agreement with the Flux Tube model and slightly above the only lattice prediction (see Table 5.1). In the exotic sector, the lightest state is given by 0^{--}, with mass 2.3 GeV. Although there are also hybrid states with explicit strangeness, e.g. $s\bar{u}g$, predictions for them are not shown since the effect from the u/s quark mass difference is small.

5.2.3 Heavy hybrid mesons

Table 5.5 shows the results for the $c\bar{c}g$ (charmonium) hybrid mesons using a charmed quark mass of 1.0 GeV. The ground state is given, again, by the 1^{+-} state, with mass 3.83 GeV, while the lightest exotic hybrid lies at 4.02 GeV. These numbers are in reasonable agreement with previous lattice and Flux Tube predictions, as listed in Table 5.1.

Note that the correction introduced in the charmed case by the g^2 terms is roughly

Table 5.4: Spectrum of $s\bar{s}g$ states. Error $\approx \pm$ 50 MeV.

J^{PC}	$M_{J^{PC}}$ (MeV) no corrections	$M_{J^{PC}}$ (MeV) with g^2 corrections	
1^{+-}	2095	2125	Ground
0^{++}	2045	2140	
2^{++}	2290	2315	
1^{++}	2325	2420	
1^{-+}	2350	2395	Exotic
0^{--}	2270	2300	Exotic
1^{-+}	2440	2485	Exotic
1^{-+}	2760	2820	Exotic
3^{-+}	2995	3030	Exotic

Table 5.5: Spectrum of $c\bar{c}g$ states. Error $\approx \pm$ 50 MeV.

J^{PC}	$M_{J^{PC}}$ (MeV) no corrections	$M_{J^{PC}}$ (MeV) with g^2 corrections	
1^{+-}	3310	3830	Ground
0^{++}	3295	3945	
2^{++}	3410	3965	
1^{++}	3450	4100	
1^{-+}	3545	4020	Exotic
0^{--}	3510	4020	Exotic
1^{-+}	3590	4155	Exotic
1^{-+}	3985	4565	Exotic
3^{-+}	4065	4615	Exotic

500 to 600 MeV, significantly higher than in the lighter hybrid systems where the average corrections are 25 to 50 MeV. This large effect arises from the hyperfine correction to the quark and anti-quark self-energies (see Eqs. (4.12, 5.7)), which is enhanced for heavier quark masses as discussed further in Ref. (10). Related, and as illustrated in Fig. 5.4, the charmonium hybrid spectrum now has a slightly different level ordering from the lighter hybrid spectra.

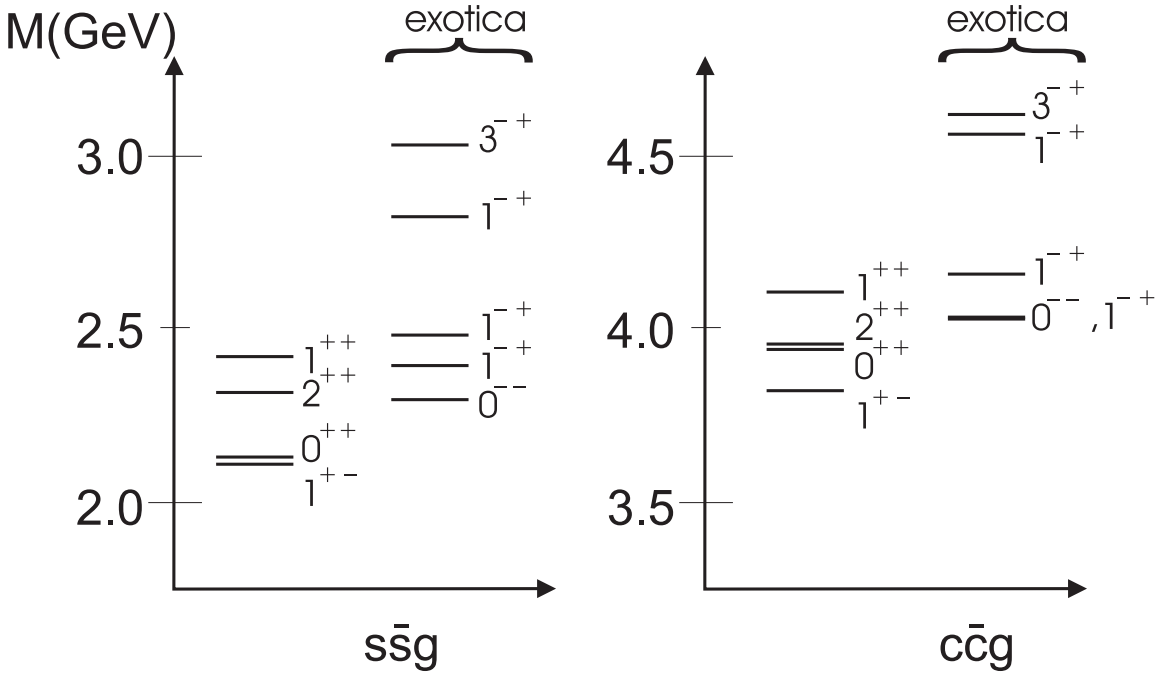

Figure 5.4: Low lying $s\bar{s}g$ and $c\bar{c}g$ spectra.

5.2.4 Sensitivity to potential and parameters

One of the key findings using the Cornell potential is that the mass of the lightest hybrid, especially the exotic 1^{-+}, is above 2 GeV. Because of the ramifications of this result for exotic state searches, an interaction sensitivity study has been performed by varying both potential forms and parameters.

First, the parameters in the Cornell potential were varied to obtain a lower bound for the predicted exotic hybrid mass. Results are shown in Table 5.6 for different

Coulomb potential parameters, α_s, and string tensions, σ, found in the literature. For any combination of values consistent with previous studies (6; 8; 10; 11) it was not possible to reduce the light hybrid mass to 1600 MeV. In particular, $0.0 \leq \alpha_s \leq 0.4$ and 367 MeV $\leq \sqrt{\sigma} \leq$ 424 MeV were tried. Indeed, to obtain a hybrid mass as low as 1600 MeV required an unphysical $\sqrt{\sigma}$ =262 MeV.

Table 5.6: Calculated light and charmonium hybrid 1^{-+} masses, in GeV, using different interactions.

potential/parameters	$I = 1$ $u\bar{d}g$ hybrid	$c\bar{c}g$ hybrid
Cornell [Eq. (3.6)]		
$\sqrt{\sigma} = 367\,\text{MeV},\ \alpha_s = 0.4$	2220	4155
$\sqrt{\sigma} = 367\,\text{MeV},\ \alpha_s = 0.2$	2390	4415
$\sqrt{\sigma} = 367\,\text{MeV},\ \alpha_s = 0.0$	2540	4645
$\sqrt{\sigma} = 424\,\text{MeV},\ \alpha_s = 0.4$	2555	4525
Renormalized [Eq. (3.9)]		
$m_g = 526\,\text{MeV}$	2705	4730
$m_g = 607\,\text{MeV}$	3010	5130

Table 5.6 also lists predictions for the confining potential given by Eq. (3.9) for values of the parameter $m_g = \sqrt{8\pi\sigma/12.25}$ corresponding to the two different Cornell string tensions σ but with the same current quark masses (m_u = 5 MeV, m_c = 1 GeV). Note that this interaction yields $u\bar{d}g$ and $c\bar{c}g$ hybrids that are heavier than those given by the Cornell potential. Most significantly, this potential also predicts the lightest exotic hybrid has mass above 2 GeV. If m_c = 0.85 GeV is used, which provides a reasonable description of the charmonium spectrum, the 1^{-+} $c\bar{c}g$ mass decreases to 4815 MeV for m_g = 607 MeV.

5.3 Searching for hybrid mesons

Discovering exotic hadrons is a major goal motivating the Jefferson Lab 12 GeV upgrade and is also being actively pursued by other collaborations and facilities, such as Babar, Belle, RHIC, etc. For low energy investigations of light quark exotic systems

there is, unfortunately, no clean energy scale demarcation, since Λ_{QCD} governs the momentum distributions in light mesons and the strange quark mass is of the same order of magnitude. The obvious detection strategy is therefore to perform statistically accurate cross sections measurements to extract partial wave amplitudes with explicitly exotic quantum numbers not accessible to ordinary $q\bar{q}$ states. However for (hidden) exotica with conventional meson quantum numbers, it will be difficult to establish their nature. Note certain Flux Tube model (39) and lattice predictions indicate that p-wave hybrid mesons prefer to decay to hadron pairs with one hadron also having a p-wave, rather than to two s-wave hadrons with a relative motion p-wave, e.g. ηh_1 in an s-wave as opposed to $\pi\pi$ in a p-wave. It will be interesting to check this prediction experimentally.

More germane to the results of this dissertation are high energy experiments where novel tests can be conducted based on the scale separation provided by either the high beam energy or the heavy quark mass. This is discussed in the next two subsections.

5.3.1 Application of dimensional counting rules

Dimensional counting rules (49) predict a power-law production cross section behavior for a given state at asymptotically high energies. They are based on the requirement that in forming a bound state with an energetic quark, the other partons must acquire very small relative momenta consistent with the production hadron's internal momentum distribution. This becomes highly unlikely in energetic collisions and therefore the production cross section falls as a power law, with the exponent increasing with increasing minimum number of constituents. For a hidden hybrid, the wavefunction has the Fock space expansion

$$|\psi\rangle = \beta_1|c\bar{c}\rangle + \beta_2|c\bar{c}g\rangle + \cdots \tag{5.13}$$

where the quantum numbers are conventional but the first coefficient β_1 is presumably small. Therefore the power-law behavior will reveal the second term in this series and permit distinguishing this exotic meson from ordinary $c\bar{c}$ charmonium (same for bottomonium). To be specific, the following discussion is focused on the recently discovered $\psi(4260)$, whose nature is currently under debate. The same remarks apply to any other hidden hybrid meson candidate.

Inclusive production First consider the inclusive production reaction $e^-e^+ \to \psi + X$. The virtual photon fragments into a $c\bar{c}$ pair, each carrying half of the total center of mass momentum and therefore each has an energy equal to the beam energy E_{beam} (in a symmetric collider). The dimensional counting rules apply in the limit in which the produced particle's energy approaches its threshold value, that is,

$$x = \frac{E_\psi}{E_{beam}} \to 1 \ . \tag{5.14}$$

In this limit, the power law behavior for a conventional charmonium state is $1 - x$ and for a hybrid state with a minimum of one more gluon constituent in the leading wavefunction, $(1-x)^3$ (50). That is, as the ψ is produced with more energy (this can be determined kinematically), the production cross section decreases linearly towards the kinematical endpoint where the ψ has the maximum available energy. Note that the hybrid production cross section decreases even more rapidly as a cubic polynomial. With a sufficient number of events this can be documented experimentally.

Exclusive production Bodwin, Braaten and Lee (51) have recently examined the reaction $e^-e^+ \to \psi\psi$. Their study focused on the ground state J/ψ, but their arguments also apply to the production of excited vector charmonia or a J/ψ accompanied by a $\psi(4260)$. They studied $\psi\psi$ production as a function of the (small) variable (m_c is the charmed quark mass)

$$r = \frac{m_c}{E_{beam}}$$

and find in the limit $r \to 0$, the differential cross section at fixed angle is constant. However, a straight-forward counting rule application predicts the production cross section is suppressed by a power of s or, equivalently, two powers of r, if one of the two produced hadrons is predominantly a hybrid meson, that is

$$\frac{d\sigma}{d\cos\theta} \simeq \text{constant} , \quad \text{for } c\bar{c} \tag{5.15}$$

$$\frac{d\sigma}{d\cos\theta} \simeq \frac{\text{constant}}{r^2} , \quad \text{for } c\bar{c}g . \tag{5.16}$$

Establishing this behavior only requires measuring double charmonium production at three sufficiently high energies. For non-vector mesons both cross sections are further suppressed by additional powers of r, but the extra r^2 signature always marks the presence of one more constituent, and therefore tags the hybrid meson. This argument also applies to the production of light hybrids in high-energy electron-positron colliders.

Finally, note that the power-law predictions are modified by QCD logarithms at very high energies and that in the strict limit $r \to 0$ or $x \to 0$, any $c\bar{c}$ admixture in the wavefunction would dominate production. However for current, available low energies, the production will still be dominated by the hybrid component if $\beta_1 << \beta_2$, i.e. if a predominantly pure hybrid state is found.

5.3.2 Distinguishing the hybrid from charmonium

In this subsection a novel method applicable to the decay of heavy quarkonium is proposed, that enables identifying a new state as either a radial excitation of conventional charmonium or a hybrid state. The method is based upon two key points.

First, note that, due to the gluon mass gap scale, a conventional $q\bar{q}$ ground state (e.g. a well established J/ψ or Υ, etc.) is lighter than a $q\bar{q}g$ ground state hybrid with the same flavor. Indeed, the ground state hybrid mass is more comparable to a radially excited quarkonium state. For example in the CGH approach the $\psi(4s)$ and

the ground state vector $c\bar{c}g$ state have similar masses. Now different eigenstates of a hermitian Hamiltonian are orthogonal with the nth radial excited state having $n-1$ nodes. Therefore, even though the total energies (masses) are similar, the relative momentum distribution of the quarks in excited charmonium looks quite different from the quark momentum distribution in the ground state hybrid (see Figs. 5.5 and 5.6).

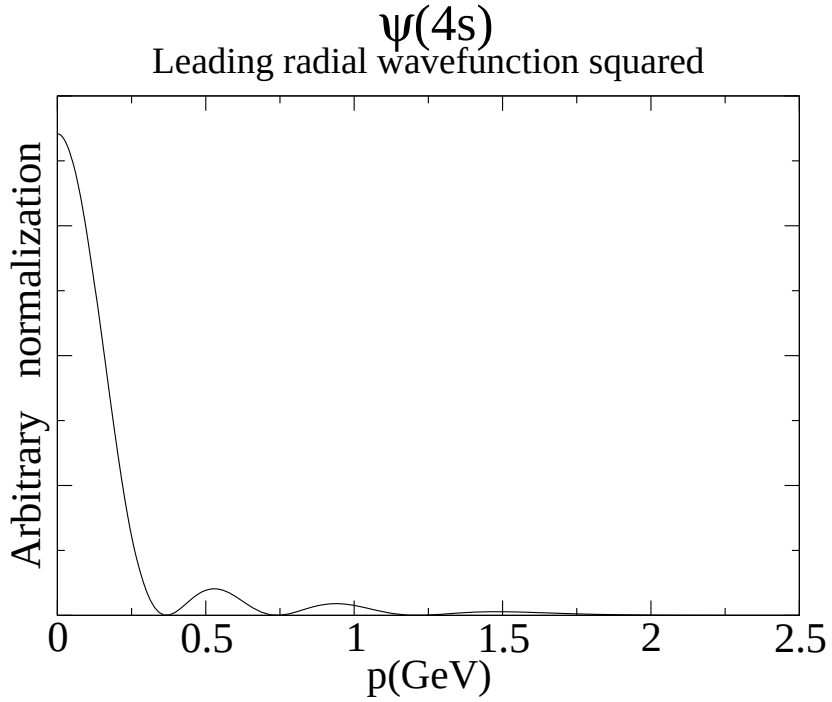

Figure 5.5: Probability density, $|\psi(p)|^2$, for the 4s charmonium state. This is the relative $c\bar{c}$ quark momentum distribution.

The second point involves the Franck-Condon (FC) principle widely used in molecular physics. Franck and Condon were the first to appreciate that molecular electronic transitions proceed too rapidly for the much heavier nuclei to respond. The FC principle is applicable whenever there is a mass scale separation between different particles. In the context of quarkonium this means that the light fields (pions, gluons, etc.) quickly rearrange and the heavy quarks do not appreciably change their momentum

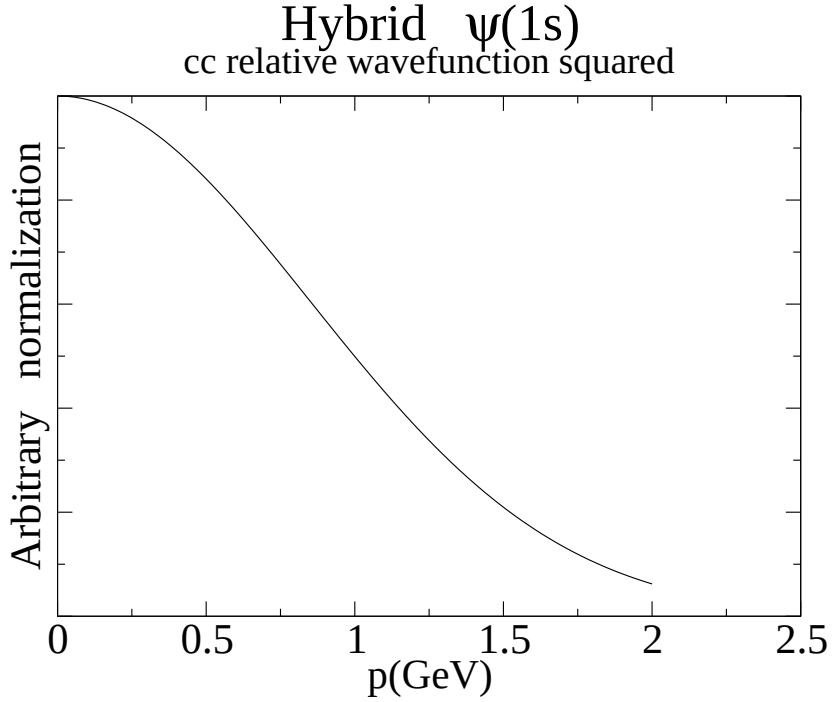

Figure 5.6: Typical quark relative momentum distribution in a $c\bar{c}g$ hybrid state with a mass near 4300 MeV. The extra mass energy, relative to a $c\bar{c}$ J/ψ, corresponds to gluon field excitations in collective models such as the Flux Tube approach or in the quasi-particle (gluon) mass gap in the constituent picture, but not in nodal radial excitation for the relative $c\bar{c}$ motion (compare to the radially excited charmonium distribution in Fig. 5.5).

distribution in the decay. Hence, the relative momentum between the decay products directly correlates with the quark momentum distribution in the parent quarkonium. Unfortunately in the simplest 2-body decays such as

$$\psi(ns) \to D\bar{D}, \quad \Upsilon(ns) \to B\bar{B}$$

the FC constraint is not relevant since in the center of mass frame the momentum of the final products is fixed. This leads to smaller wavefunction overlaps suppressing

the decay somewhat. However in 3-body decays such as

$$\psi(ns) \to D\bar{D}\pi, \quad \Upsilon(ns) \to B\bar{B}\pi \ ,$$

the FC constraint applies. The first reaction can be employed to study the recently discovered $\psi(4260)$. The second will be useful in an envisioned Belle collaboration measurement to establish whether this excited bottomonium state is the predicted quark model 5s meson state.

Thus, the relative momentum distribution between the D and $\bar{D}$ mesons in the $D\bar{D}\pi$ system mirrors the momentum distribution of the quarks in the parent ψ meson. Since the hybrid ground state wavefunction does not have a node, the resulting momentum distribution for the $D\bar{D}$ subsystem is also node-less and thus smoother than that for a conventional radially excited charmonium. Multiplying by the relevant phase space distribution for this decay, yields the momentum distribution in Fig. 5.7 that can be observed experimentally in the heavy-quark limit. The maximum is in the mid-momentum region where phase-space is larger and the wavefunction is near a local maximum.

However, since quarks are not infinitely heavy, the FC signature is modified due to the recoil of the quarks in the D meson, yielding a different momentum distribution. For example, taking a quark relative momentum between 150 and 200 MeV, one obtains the $c\bar{c}g$ momentum distribution illustrated in Fig. 5.8 for the ground state vector hybrid, and the smeared final state $D\bar{D}$ momentum distribution plotted in Fig. 5.9 for radially excited charmonium. As can be seen, even after smearing, there is still residual structure information adjacent to the central peak for radially excited charmonium that is reminiscent of its parent charmonium wavefunction behavior, in sharp contrast to the smooth, bell-shaped hybrid distribution.

Is it, therefore, advocated to analyze the $D\bar{D}$ and $B\bar{B}$ relative momentum distributions in $D\bar{D}\pi$ and $B\bar{B}\pi$ decays of highly excited quarkonia. Additional final state pions or other light particles do not alter these arguments (but restrict somewhat

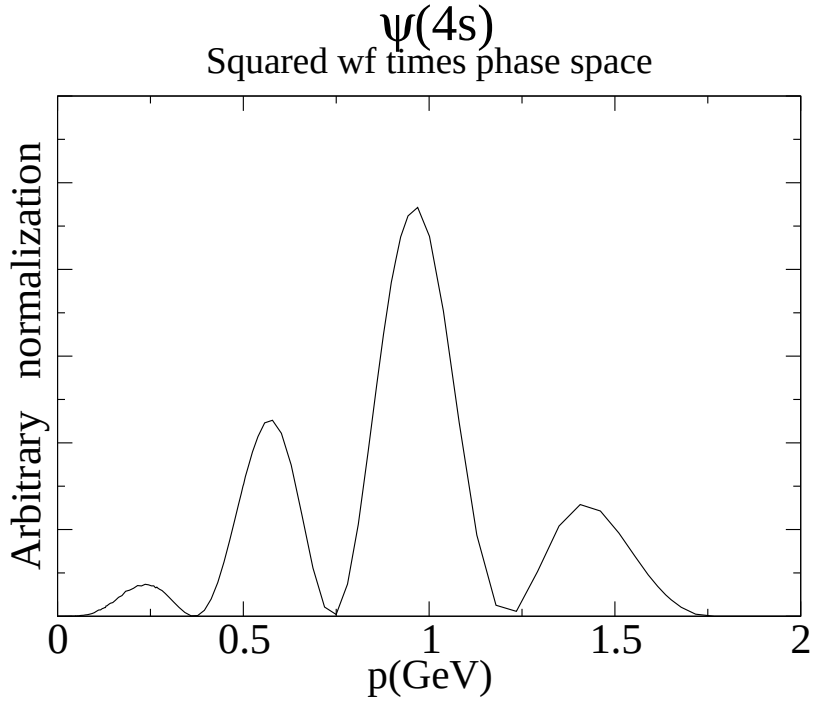

Figure 5.7: Momentum distribution of Fig. 5.5 multiplied by the phase space for the decay $\psi(4260) \to D\bar{D}\pi$. This is the probability density for finding a $D\bar{D}\pi$ state with relative $D\bar{D}$ momentum p according to the Franck-Condon principle in the heavy-quark limit. This signature will be more robust for the related bottomonium process $\Upsilon(5s) \to B\bar{B}\pi$.

the available phase space), so there are several other possible final state channels to search.

5.4 Discussion and Conclusions

A key CGH model prediction is that the lightest hybrid mass is 2.1 GeV, with the lightest 1^{-+} exotic state slightly above 2.2 GeV. Lattice and Flux Tube calculations yield a mass of at least 1.8 GeV for the 1^{-+}, except Ref. (37) which predicts a mass around 1.7 GeV. Thus, with exception to this last work, the composite model analyses appear to preclude the possibility of the reported 1^{-+} exotica, $\pi_1(1400)$ and $\pi_1(1600)$, being hybrid mesons. If this is correct, one should investigate other

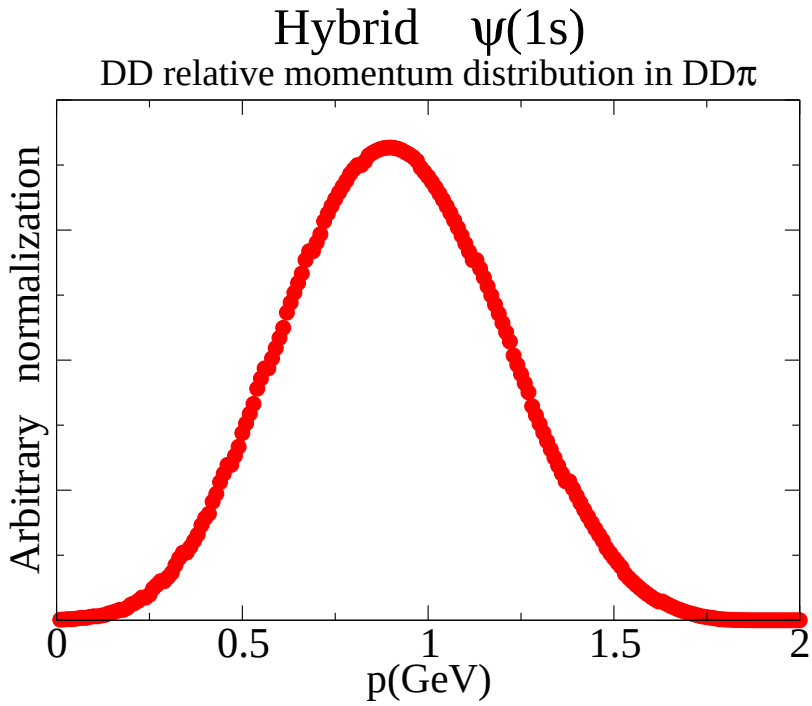

Figure 5.8: The relative momentum distribution of the $D\bar{D}$ pair in the $D\bar{D}\pi$ final state for a charmed hybrid meson with momentum distribution given in Fig. 5.6. The distribution of the final products has a smooth bell shape in sharp contrast to the radially excited quarkonium distribution in Fig. 5.9.

structures for those two hadrons, such as tetraquark molecules, with both $q\overline{q}$ pairs in color singlets, or tetraquark atoms, where quark pairs are in intermediate non-singlet color states. This is investigated in the next chapter. However, if the lattice 1.7 GeV 1^{-+} prediction is robust, one can not yet exclude the observed $\pi_1(1600)$ from being a hybrid, but this still does not explain the structure of the $\pi_1(1400)$. It would be very useful to have other lattice measurements, using the same techniques as Ref. (37), to confirm or reject this result. Related, the model parameters and potential forms have been varied in order to obtain a lower bound for the predicted exotic hybrid mass which is clearly above 2 GeV.

Regarding isospin splitting, the results show an enhanced splitting from g^2 corrections. For the 0^{++} hybrid, the corrections increased the splitting from 15 to 35 MeV,

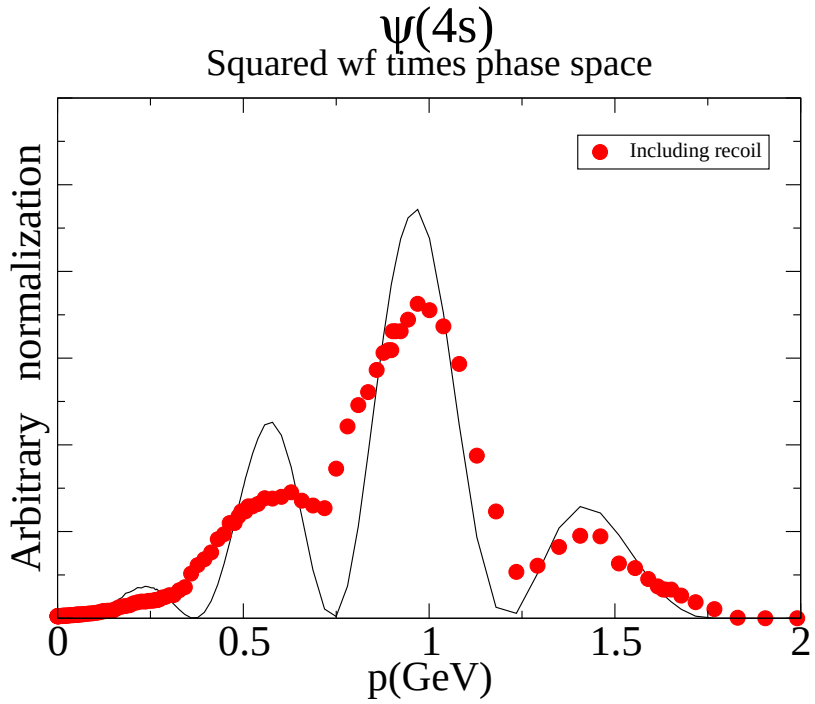

Figure 5.9: The momentum distribution in Fig. 5.7 (solid line) and the distribution (dots) obtained averaging over a 150 MeV spread to approximate the actual quark momentum distribution in the D meson. The experimental signal, firmer for bottomonium than charmonium, is a central peak with two shoulders for the relative momentum distribution of the $B\bar{B}$ (or $D\bar{D}$) pair in the $B\bar{B}\pi$ (or $D\bar{D}\pi$) final state. These adjacent enhancements identify the resonance as a radially excited quarkonium state as opposed to a hybrid meson.

the maximum increase in the light hybrid spectrum.

In the strange sector, the predicted lightest non-exotic hybrid mass is 2.125 GeV, while the lightest exotic mass is 2.30 GeV. These values compare reasonably well with Flux Tube (39; 40; 41) and, slightly lighter, lattice (37) results. For the charmed sector, the predictions of 3.83 GeV for the lightest hybrid and 4.02 GeV for the lowest exotic are also in good agreement with several other lattice and Flux Tube studies (see Table 5.1).

As mentioned above, the different g^2 corrections produced an overall small effect, about the same order as the Monte Carlo error. However, the hyperfine correction

becomes important for heavier quark mass. In the charmed sector, this correction added about 500 to 600 MeV to the hybrid mass. Lastly, note the level ordering of the exotic isoscalar $u\bar{u}g$ and $s\bar{s}g$ spectra are the same, 0^{--}, 1^{-+}, 1^{-+}, 1^{-+} and 3^{-+}, but slightly different than the exotic $c\bar{c}g$ system, where the 0^{--} and lowest 1^{-+} are degenerate. This is a consequence of the enhanced charmonium self-energy from the hyperfine interaction.

Finally, both low and high energy scenarios for observing hybrid mesons were discussed. For low energy studies involving light quark systems, dimensional counting rules predict specific power-law behaviors for distinguishing between production of conventional and hybrid mesons. For high energy investigations of heavy quark systems, the Frank-Condon principle provides a useful constraint on the final state momentum distributions which should assist experimentalist in identifying heavy hybrid systems.

In summary, lattice, Flux Tube and the $H_{\rm eff}$ many-body approach all predict similar hybrid spectra and that the lightest 1^{-+} exotic hybrid meson mass is near 2 GeV. This composite model agreement indicates that the $\pi_1(1600)$ is not a hybrid meson but has an alternative structure. If true and if the $\pi_1(1600)$ exists, it is more likely a tetraquark system, either a $(q\bar{q})$ $(q\bar{q})$ meson molecule or an exotic $qq\bar{q}\bar{q}$ atom. In the next chapter, the present model will be applied to light and heavy tetraquark systems.

Chapter 6

Tetra-quarks

The same Hamiltonian used in this work has been previously considered (6; 8; 10; 11) to study the two-body meson and glueball systems by diagonalizing H_{eff} through the Tamm-Dancoff and Random Phase Approximations. In last chapter, it was applied to study hybrid mesons but, given the complexity of the three-body problem, the variational principle was used instead. Now, this program is continued and the tetra-quark system is studied, also, by means of the variational principle. This time, as it is a first study of the tetra-quark problem, corrections of order g^2 are neglected (in analogy to what was done in the hybrid case). Note that the inclusion of those corrections in the four-body problem represents an even more challenging task, since there are more interactions and, thus, more integrals to calculate. Further, the introduction of an additional variational parameter, as described below, also increases the number of calculations needed to obtain their correct optimization. Finally, given that the central focus is now on light tetra-quarks, next order corrections are expected to be small, based on the results of the last chapter.

6.1 Construction of tetra-quarks

6.1.1 Wavefunction ansatz and quantum numbers

Examining the color algebra of the system reveals there are two independent tetra-quark singlet states: $3 \otimes \overline{3} \otimes 3 \otimes \overline{3} = 27 \oplus 10 \oplus \overline{10} \oplus 8 \oplus 8 \oplus 8 \oplus 8 \oplus 1 \oplus 1$. But they can be obtained in four different ways, depending on the intermediate color states: the singlet scheme (or molecule), the octet scheme , the triplet scheme and the sextet scheme (see Fig. 6.1).

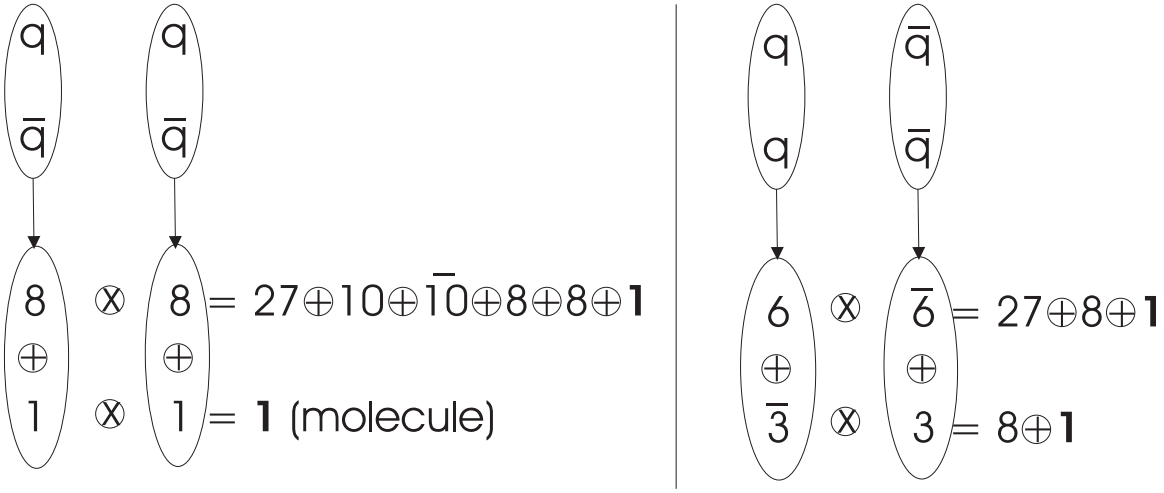

Figure 6.1: Singlets can be obtained via four different schemes (only two are independent): octet, singlet (or molecule), sextet and triplet.

Working in the tetra-quark center of momentum system, denote the momenta of the quarks by $\mathbf{q_1}$ and $\mathbf{q_3}$, and those of the anti-quarks by $\mathbf{q_2}$ and $\mathbf{q_4}$ (this is for the singlet or octet schemes; for the triplet or sextet configurations take $\mathbf{q_1}$ and $\mathbf{q_2}$ for the quarks and $\mathbf{q_3}$ and $\mathbf{q_4}$ for the anti-quarks). Analogously to what was done with the hybrid system, new coordinates are defined, $\boldsymbol{q}_A = \frac{\boldsymbol{q}_1 - \boldsymbol{q}_2}{2}$, $\boldsymbol{q}_B = \frac{\boldsymbol{q}_3 - \boldsymbol{q}_4}{2}$ and $\boldsymbol{q}_I = \frac{\boldsymbol{q}_3 + \boldsymbol{q}_4}{2} - \frac{\boldsymbol{q}_1 + \boldsymbol{q}_2}{2}$, and the following wavefunction ansatz is proposed:

$$|\Psi^{JPC}\rangle = \iiint \frac{d\boldsymbol{q}_A}{(2\pi)^3}\frac{d\boldsymbol{q}_B}{(2\pi)^3}\frac{d\boldsymbol{q}_I}{(2\pi)^3}\Phi^{JPC}_{\lambda_1\lambda_2\lambda_3\lambda_4}(\boldsymbol{q}_A, \boldsymbol{q}_B, \boldsymbol{q}_I) \\ R^{\mathcal{C}_1\mathcal{C}_2}_{\mathcal{C}_3\mathcal{C}_4} B^\dagger_{\lambda_1\mathcal{C}_1}(\boldsymbol{q}_1) D^\dagger_{\lambda_2\mathcal{C}_2}(\boldsymbol{q}_2) B^\dagger_{\lambda_3\mathcal{C}_3}(\boldsymbol{q}_3) D^\dagger_{\lambda_4\mathcal{C}_4}(\boldsymbol{q}_4)|\Omega\rangle, \tag{6.1}$$

where the expression for the matrix $R^{\mathcal{C}_1\mathcal{C}_2}_{\mathcal{C}_3\mathcal{C}_4}$ depends on the specific color scheme chosen. The space part of the wavefunction, Φ, is determined through an explicit choice of the angular momentum coupling scheme,

$$\begin{aligned}\Phi^{JPC}_{\lambda_1\lambda_2\lambda_3\lambda_4}(\boldsymbol{q}_A,\boldsymbol{q}_B,\boldsymbol{q}_I) &= F^{JPC}(q_A,q_B,q_I)Y^{m_A}_{l_A}(\hat{\boldsymbol{q}}_A)Y^{m_B}_{l_B}(\hat{\boldsymbol{q}}_B)Y^{m_I}_{l_I}(\hat{\boldsymbol{q}}_I)\\ &\langle\frac{1}{2}\frac{1}{2},\lambda_1\lambda_2|S_A\lambda_A\rangle\langle S_A l_A,\lambda_A m_A|J_A M_A\rangle\langle\frac{1}{2}\frac{1}{2},\lambda_3\lambda_4|S_B\lambda_B\rangle\\ &\langle S_B l_B,\lambda_B m_B|J_B M_B\rangle\langle J_A J_B,M_A M_B|S\lambda\rangle\langle S l_I,\lambda m_I|JM\rangle,\end{aligned} \tag{6.2}$$

where the radial part is chosen to be a Gaussian with variational parameters $\alpha_A,\alpha_B,\alpha_I$,

$$F(q_A,q_B,q_I,\alpha_A,\alpha_B,\alpha_I) = e^{-\frac{q_A^2}{\alpha_A^2}-\frac{q_B^2}{\alpha_B^2}-\frac{q_I^2}{\alpha_I^2}}, \tag{6.3}$$

when treating s-wave states and a Gaussian multiplied by q_i^2/α_i^2 $(i=A,B,I)$ corresponding to $l_i=1$, when treating p-wave states.

6.1.2 Variational equations of motion

The tetra-quark mass is then given, according to the variational principle, by

$$\begin{aligned}M_{JPC} &\leq \frac{\langle\Psi^{JPC}|H_{\rm eff}|\Psi^{JPC}\rangle}{\langle\Psi^{JPC}|\Psi^{JPC}\rangle}\\ &= M_{self}+M_{q-q}+M_{\bar{q}-\bar{q}}+M_{q-\bar{q}}+M_{annih},\end{aligned} \tag{6.4}$$

where the subscripts indicate the source of each contribution; the self-energy of the pair of quarks and anti-quarks, the qq, $\bar{q}\bar{q}$ and $q\bar{q}$ scattering, and the $q\bar{q}$ annihilation, respectively. This is diagrammatically represented in Fig. 6.2. This equation of motion is given, in the center of momentum system, by twelve dimensional integrals, which are numerically solved using the Monte-Carlo type VEGAS code (47), as it was used in the hybrid meson case. But this time, due to the increased complexity of the problem, the number of points used to calculate the integrals is increased to 50 million, as necessary to achieve convergence. The full contributions are expressed by

$$M_{\rm self} = \sum_{i=1}^{4} \iiint \frac{d\boldsymbol{q}_1\, d\boldsymbol{q}_2\, d\boldsymbol{q}_3}{(2\pi)^9} \Phi^{JPC\dagger}_{\lambda_1\lambda_2\lambda_3\lambda_4}(\boldsymbol{q}_1,\boldsymbol{q}_2,\boldsymbol{q}_3)\Phi^{JPC}_{\lambda_1\lambda_2\lambda_3\lambda_4}(\boldsymbol{q}_1,\boldsymbol{q}_2,\boldsymbol{q}_3)E_i(\boldsymbol{q}_i), \quad (6.5)$$

where

$$E_i(\boldsymbol{q}_i) = m_i \sin\Theta(\boldsymbol{q}_i) + \boldsymbol{q}_i \cos\Theta(\boldsymbol{q}_i) + \quad (6.6)$$
$$\int d\boldsymbol{k}\, V(\boldsymbol{k}) \left[\sin\Theta(\boldsymbol{q}_i)\sin\Theta(\boldsymbol{q}_i+\boldsymbol{k}) + \cos\Theta(\boldsymbol{q}_i)\cos\Theta(\boldsymbol{q}_i+\boldsymbol{k})\hat{\boldsymbol{q}}_i\cdot(\boldsymbol{q}_i \hat{+} \boldsymbol{k})\right],$$

$$\begin{aligned} M_{q-q} &= \iiint\!\!\int \frac{d\boldsymbol{q}_1\, d\boldsymbol{q}_2\, d\boldsymbol{q}_3\, d\boldsymbol{k}}{(2\pi)^{12}} V(\boldsymbol{k}) u^{\dagger}_{\lambda_1'}(\boldsymbol{q}_1+\boldsymbol{k}) u_{\lambda_1}(\boldsymbol{q}_1) u^{\dagger}_{\lambda_3'}(\boldsymbol{q}_3-\boldsymbol{k}) u_{\lambda_3}(\boldsymbol{q}_3) \\ &\quad \Phi^{JPC\dagger}_{\lambda_1\lambda_2\lambda_3\lambda_4}(\boldsymbol{q}_1,\boldsymbol{q}_2,\boldsymbol{q}_3)\Phi^{JPC}_{\lambda_1\lambda_2\lambda_3\lambda_4}(\boldsymbol{q}_1+\boldsymbol{k},\boldsymbol{q}_2,\boldsymbol{q}_3-\boldsymbol{k}), \end{aligned} \quad (6.7)$$

$$\begin{aligned} M_{\bar{\boldsymbol{q}}-\bar{\boldsymbol{q}}} &= \iiint\!\!\int \frac{d\boldsymbol{q}_1\, d\boldsymbol{q}_2\, d\boldsymbol{q}_3\, d\boldsymbol{k}}{(2\pi)^{12}} V(\boldsymbol{k}) v^{\dagger}_{\lambda_2}(\boldsymbol{q}_2) v_{\lambda_2'}(\boldsymbol{q}_2+\boldsymbol{k}) v^{\dagger}_{\lambda_4}(\boldsymbol{q}_4) v_{\lambda_4'}(\boldsymbol{q}_4-\boldsymbol{k}) \\ &\quad \Phi^{JPC\dagger}_{\lambda_1\lambda_2\lambda_3\lambda_4}(\boldsymbol{q}_1,\boldsymbol{q}_2,\boldsymbol{q}_4)\Phi^{JPC}_{\lambda_1\lambda_2\lambda_3\lambda_4}(\boldsymbol{q}_1,\boldsymbol{q}_2+\boldsymbol{k},\boldsymbol{q}_4-\boldsymbol{k}), \end{aligned} \quad (6.8)$$

$$\begin{aligned} M_{q-\bar{q}} &= \iiint\!\!\int \frac{d\boldsymbol{q}_1\, d\boldsymbol{q}_2\, d\boldsymbol{q}_3\, d\boldsymbol{k}}{(2\pi)^{12}} V(\boldsymbol{k}) u^{\dagger}_{\lambda_1'}(\boldsymbol{q}_1+\boldsymbol{k}) u_{\lambda_1}(\boldsymbol{q}_1) v^{\dagger}_{\lambda_2'}(\boldsymbol{q}_2-\boldsymbol{k}) v_{\lambda_2}(\boldsymbol{q}_2) \\ &\quad \Phi^{JPC\dagger}_{\lambda_1\lambda_2\lambda_3\lambda_4}(\boldsymbol{q}_1,\boldsymbol{q}_2,\boldsymbol{q}_3)\Phi^{JPC}_{\lambda_1\lambda_2\lambda_3\lambda_4}(\boldsymbol{q}_1+\boldsymbol{k},\boldsymbol{q}_2-\boldsymbol{k},\boldsymbol{q}_3), \end{aligned} \quad (6.9)$$

$$\begin{aligned} M_{\rm annih} &= \iiint\!\!\int \frac{d\boldsymbol{q}_1\, d\boldsymbol{q}_2\, d\boldsymbol{q}_3\, d\boldsymbol{k}}{(2\pi)^{12}} V(\boldsymbol{q}_1+\boldsymbol{q}_2) u^{\dagger}_{\lambda_1'}(\boldsymbol{q}_1+\boldsymbol{k}) v_{\lambda_2'}(\boldsymbol{q}_2-\boldsymbol{k}) v^{\dagger}_{\lambda_2}(\boldsymbol{q}_2) u_{\lambda_2}(\boldsymbol{q}_2) \\ &\quad \Phi^{JPC\dagger}_{\lambda_1\lambda_2\lambda_3\lambda_4}(\boldsymbol{q}_1,\boldsymbol{q}_2,\boldsymbol{q}_3)\Phi^{JPC}_{\lambda_1\lambda_2\lambda_3\lambda_4}(\boldsymbol{q}_1+\boldsymbol{k},\boldsymbol{q}_2-\boldsymbol{k},\boldsymbol{q}_3). \end{aligned} \quad (6.10)$$

The interest is now in calculating the ground state masses as well as the 1^{-+} exotic states of the light tetra-quarks. Also, the present model can be used to compare the 1^{++} and 1^{--} charmed tetra-quarks predictions to the X(3872) and Y(4260) particles,

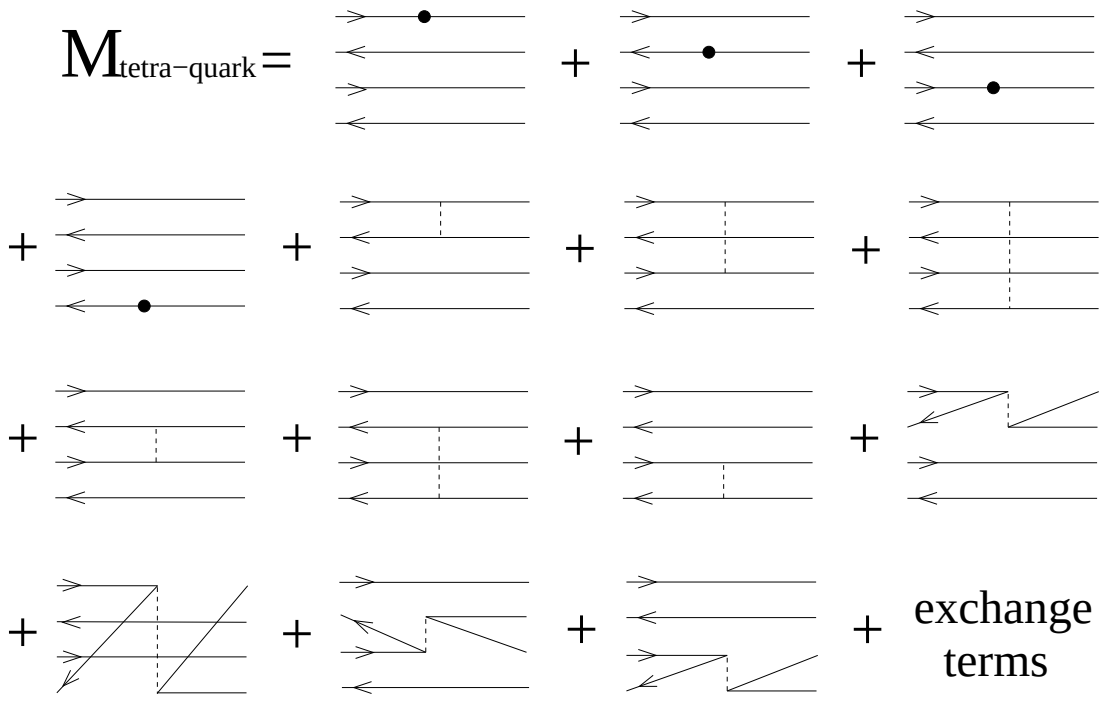

Figure 6.2: Diagrams for $\langle \Psi_{4q} | H | \Psi_{4q} \rangle$

which have been suggested to be tetra-quarks (52; 53; 54). In this formulation there are three angular momenta, l_A, l_B and l_I, representing the relative momenta of cluster A, cluster B and of the inter-cluster system, respectively. Consequently, the ground state must have three s-waves, while the 1^{-+} states have one p-wave and two s-waves.

6.2 Results: Tetra-quark Spectrum

6.2.1 Light tetra-quarks

For the light tetra-quark calculations, $m = 5$ MeV (48) is used for the u/d current quark mass. Results are listed in Tables 6.1 and 6.2, which show the ground state is the non-exotic vector state 1^{++}, in the singlet-color scheme, with isospin 1; its mass is found around 1.2 GeV. In general (both in exotic and non-exotic cases), any state is lightest in the singlet-color scheme; this is a consequence of the cancellation of most inter-cluster interactions in this scheme, due to vanishing color factors for those

Table 6.1: Spectrum of light non-exotic tetra-quark states. Error $\approx \pm$ 50 MeV.

$(q\bar{q})_8(q\bar{q})_8$	I=2	I=1(1x1)	I=1(1x0)	I=0(1x1)	I=0(0x0)
0^{++}	1.662	-	1.817	1.691	1.909
1^{+-} (s_{13}=1 or s_{24}=1)	1.662	-	1.817	1.691	1.909
0^{++} (s_{13}=1 and s_{24}=1)	1.713	-	1.801	1.677	1.837
1^{++} (s_{13}=1 and s_{24}=1)	-	1.708	1.746	-	-
2^{++} (s_{13}=1 and s_{24}=1)	1.653	-	1.802	1.724	1.898
$(q\bar{q})_1(q\bar{q})_1$	I=2	I=1(1x1)	I=1(1x0)	I=0(1x1)	I=0(0x0)
0^{++}	1.418	-	1.418	1.417	1.418
1^{+-} (s_{13}=1 or s_{24}=1)	1.418	-	1.418	1.417	1.418
0^{++} (s_{13}=1 and s_{24}=1)	1.282	-	1.282	1.283	1.282
1^{++} (s_{13}=1 and s_{24}=1)	-	1.215	1.215	-	-
2^{++} (s_{13}=1 and s_{24}=1)	1.351	-	1.351	1.350	1.351
$(qq)_{\bar{3}}(\bar{q}\bar{q})_3$	I=2	I=1(1x1)	I=1(1x0)	I=0(1x1)	I=0(0x0)
0^{++}	-	-	-	-	1.733
1^{++} (s_{12}=1 or s_{34}=1)	-	-	1.770	-	-
0^{++} (s_{12}=1 and s_{34}=1)	1.724	1.913	-	1.997	-
1^{++} (s_{12}=1 and s_{34}=1)	1.728	1.935	-	2.017	-
2^{++} (s_{12}=1 and s_{34}=1)	1.721	1.897	-	1.970	-
$(qq)_6(\bar{q}\bar{q})_{\bar{6}}$	I=2	I=1(1x1)	I=1(1x0)	I=0(1x1)	I=0(0x0)
0^{++}	1.634	1.758	-	1.812	-
1^{+-} (s_{12}=1 or s_{34}=1)	-	-	1.694	-	-
0^{++} (s_{12}=1 and s_{34}=1)	-	-	-	-	1.731
1^{++} (s_{12}=1 and s_{34}=1)	-	-	-	-	1.749
2^{++} (s_{12}=1 and s_{34}=1)	-	-	-	-	1.710

interactions, contrary to what happens in the other schemes, where the color factors never cancel.

In the case of exotic 1^{-+} states, the triplet and sextet color configurations can only exist if the states are a superposition of, at least, two states with defined quantum numbers $(l_A, l_B, l_I, s_A, s_B, s_I)$. This is due to the condition that, if constituted by only one state, then these color schemes require $C = P$ in a given J^{PC} state, thus forbidding the 1^{-+} exotic.

As indicated in Table 6.2, the lightest 1^{-+} is around 1.4 GeV, in the singlet scheme, as expected. But this is not the lightest exotic; the 0^{--} is found below, at 1.35 GeV, in its isospin 2, singlet scheme state.

Table 6.2: Spectrum of light exotic tetra-quark states. Error $\approx \pm$ 50 MeV.

$(q\bar{q})_8(q\bar{q})_8$	I=2	I=1(1x1)	I=1(1x0)	I=0(1x1)	I=0(0x0)
1^{-+} (l_I=1)	-	2.196	2.236	-	-
1^{-+} ($l_A = s_A$=1 or $l_B = s_B$=1)	2.105	2.149	2.201	2.200	2.209
1^{-+} ($l_A = s_B$=1 or $l_B = s_A$=1)	2.159	2.199	2.236	2.232	2.239
0^{--} ($l_I = s_A$=1 or $l_I = s_B$=1)	2.119	2.113	2.152	2.101	2.149
$(q\bar{q})_1(q\bar{q})_1$	I=2	I=1(1x1)	I=1(1x0)	I=0(1x1)	I=0(0x0)
1^{-+} (l_I=1)	-	1.416	1.417	-	-
1^{-+} ($l_A = s_A$=1 or $l_B = s_B$=1)	1.795	1.797	1.797	1.797	1.797
1^{-+} ($l_A = s_B$=1 or $l_B = s_A$=1)	1.910	1.910	1.910	1.910	1.910
0^{--} ($l_I = s_A$=1 or $l_I = s_B$=1)	1.355	1.362	1.362	1.362	1.362
$(q\bar{q})_3(q\bar{q})_3$	I=2	I=1(1x1)	I=1(1x0)	I=0(1x1)	I=0(0x0)
1^{-+} (l_A=1 or l_B=1)	-	-	2.177	-	-
1^{-+} ($l_A = s_A$=1 or $l_B = s_B$=1)	-	-	-	-	2.316
1^{-+} ($l_A = s_B$=1 or $l_B = s_A$=1)	2.177	2.239	-	2.269	-
0^{--} (l_I=1 and (s_A=1 or s_B=1))	-	-	2.078	-	-
$(q\bar{q})_6(q\bar{q})_6$	I=2	I=1(1x1)	I=1(1x0)	I=0(1x1)	I=0(0x0)
1^{-+} (l_A=1 or l_B=1)	-	-	2.097	-	-
1^{-+} ($l_A = s_A$=1 or $l_B = s_B$=1)	2.014	2.056	-	2.076	-
1^{-+} ($l_A = s_B$=1 or $l_B = s_A$=1)	-	-	-	-	2.087
0^{--} (l_I=1 and (s_A=1 or s_B=1))	-	-	2.163	-	-

Table 6.3: Mass of 1^{++} ($l_A = l_B = l_I = 0, s_A = s_B = 1$) $c\bar{c}u\bar{u}$, possible configuration of X(3872). Error $\approx \pm$ 50 MeV.

m_c	$\sqrt{\sigma}$	$(c\bar{c})_1(u\bar{u})_1$	$(c\bar{u})_1(u\bar{c})_1$
1.2	0.424	3.741	3.869
1.0	0.424	3.349	3.472
1.2	0.367	3.557	3.667
1.0	0.367	3.161	3.270

Table 6.4: Mass of 1^{--} ($l_A = 1$ or $l_B = 1, l_I = s_A = s_B = 0$) $c\bar{c}s\bar{s}$, possible configuration of Y(4262). Error $\approx \pm$ 50 MeV.

$\sqrt{\sigma}$	$(c\bar{c})_1(s\bar{s})_1$	$(c\bar{s})_1(s\bar{c})_1$
0.424	4.308	4.308
0.367	4.049	4.049

Note that for each color scheme, there are some states forbidden by symmetry of the wave-function. For example, in diquark (triplet and sextet) case, the wave function (including spin, flavor, color and angular momentum) should be antisymmetric under exchange of two quarks or two anti-quarks. For example, for 1^{-+} with $l_A = s_A = 1$, the color wavefunction between two quarks (anti-quarks) is antisymmetric under the mentioned exchange. So is the spin together with angular momentum. Therefore, to make the total wave function antisymmetric, the flavor should also be antisymmetric, i.e. isospin $0(0 \times 0)$. Due to this symmetry requirement, most states in the triplet scheme do not exist in the sextet color configuration and vice versa.

6.2.2 Heavy tetra-quarks

For the heavy tetra-quarks, different parameters sets are used, based on previous works. The results are listed in Tables 6.3 and 6.4 and correspond to the singlet color scheme, which gives the lowest masses. Note that to identify the 1^{++} state as the X(3872), the parameter set is: $m_c = 1.2GeV$ and $\sqrt{\sigma} = 0.424$. The same set is used to predict the Y(4262).

6.3 Conclusions

The key finding of this study, along with the results on hybrid mesons described in chapter 5, that the lightest hybrid 1^{-+} is around 2.1 GeV, is that the π_1 states are most likely tetra-quark states. In particular, the $\pi_1(1400)$ is strongly matched to a tetra-quark in the form of a molecule composed of two mesons (singlet color scheme), in an isospin 1 state and with an inter-cluster p-wave, with a mass of 1.4 GeV. The $\pi_1(1600)$ is about 200 MeV below the next 1^{-+} state, having a p-wave in one of the two clusters.

Regarding charmed tetra-quarks, their spectra could very well accommodate the X(3872) and Y(4262) resonances, as long as the parameter set is taken as $m_c = 1.2$ GeV and $\sqrt{\sigma} = 0.424$.

Chapter 7

Summary and Future Work

Summarizing, using the CGH model, the gap equations for the quark and gluon have been obtained and used to calculate their self-energies and condensates. Then, large-scale Monte Carlo calculations for $q\bar{q}g$ hybrid mesons and $q\bar{q}q\bar{q}$ tetraquark systems were performed.

For the hybrid meson investigation, the CGH model predicts that all $u\bar{u}g$ and $u\bar{d}g$ states have mass above 2 GeV. This is consistent with lattice and Flux Tube model predictions for light exotic 1^{-+} hybrid mesons, and strongly suggests that observed $\pi_1(1400)$ and $\pi_1(1600)$ are not hybrid mesons but have an alternative structure as argued below.

The tetraquark results clearly show that molecular states, those with an intermediate singlet color structure, $[(q\bar{q})_1 \otimes (q\bar{q})_1]_1$, are lighter than the atomic states, those with the more exotic octet, triplet or sextet color structures, $[(q\bar{q})_8 \otimes (q\bar{q})_8]_1$, $[(qq)_3 \otimes (\bar{q}\bar{q})_3]_1$ or $[(qq)_6 \otimes (\bar{q}\bar{q})_6]_1$, respectively. Most significantly, for the 1^{-+}, $I = 1$ channel the predicted lightest color octet state is above 2 GeV, while the lightest singlet scheme state is around 1400 MeV, close to the $\pi(1400)$.

Combining the above hybrid meson and tetra-quark results, with other models predictions for hybrids (all agreeing in that their mass is above $1.7\,GeV$), strongly suggests that the observed exotic π_1 states are not hybrids or exotic color configura-

tions of 4 quarks but, rather, more conventional meson-meson type molecules. This is the key conclusion of this thesis.

Also, in the charmed tetra-quark study it was found that the spectra corresponding to the $c\bar{c}u\bar{u}$ and $c\bar{c}s\bar{s}$ structures could very well accommodate the X(3872) and Y(4262) resonances, respectively.

Concerning future research, it would be interesting to study the dynamical mixing of glueball, meson, hybrid meson and tetraquark states, within the framework of the CGH model, along with the study of three-body forces (14) for the treatment of baryons. Also, this model could be used to calculate penta-quark states to help clarify the controversy regarding their existence.

Even though this model has been successful in reproducing the meson spectrum and agrees very well with lattice and Flux-Tube predictions regarding glueballs and hybrid mesons (there are not many predictions for tetra-quarks), there are still some points to improve. One is to develop a phenomenological confining kernel that very accurately reproduces the meson and lattice glueball spectra. This will allow a more robust prediction for exotic searches. Another point would be to incorporate the Faddeev-Popov determinant (FP) since it has been shown (55) that contributions from the inverse FP operator are infrared enhanced. However, this correction should not appreciably modify hadron mass predictions which are dominated by the long range (ultraviolet) part of the Coulomb confinement kernel.

Bibliography

[1] F. Karsch, Lect. Notes Phys. **583**, 209 (2002).

[2] Y. Nambu and G. Jona-Lasinio, Phys. Rev. **122**, 345 (1961).

[3] Y. Nambu and G. Jona-Lasinio, Phys. Rev. **124**, 246 (1961).

[4] N. Isgur and J. E. Paton, Phys. Rev. **D31**, 2910 (1985).

[5] A. Szczepaniak, E. S. Swanson, C.-R. Ji, and S. R. Cotanch, Phys. Rev. Lett. **76**, 2011 (1996).

[6] F. J. Llanes-Estrada and S. R. Cotanch, Phys. Rev. Lett. **84**, 1102 (2000).

[7] F. J. Llanes-Estrada and S. R. Cotanch, Phys. Lett. **B504**, 15 (2001).

[8] F. J. Llanes-Estrada and S. R. Cotanch, Nucl. Phys. **A697**, 303 (2002).

[9] F. J. Llanes-Estrada, S. R. Cotanch, P. J. de A. Bicudo, J. E. F. T. Ribeiro, and A. P. Szczepaniak, Nucl. Phys. **A710**, 45 (2002).

[10] F. J. Llanes-Estrada, S. R. Cotanch, A. P. Szczepaniak, and E. S. Swanson, Phys. Rev. **C70**, 035202 (2004).

[11] F. J. Llanes-Estrada, P. Bicudo, and S. R. Cotanch, Phys. Rev. Lett. **96**, 081601 (2006).

[12] T. D. Lee, *Particle Physics and Introduction to Field Theory*, Harwood Academic Publishers, New York, 1990.

[13] N. H. Christ and T. D. Lee, Phys. Rev. **D22**, 939 (1980).

[14] A. P. Szczepaniak and P. Krupinski, Phys. Rev. **D73**, 116002 (2006).

[15] J. Greensite and S. Olejnik, Phys. Rev. **D67**, 094503 (2003).

[16] D. Zwanziger, Phys. Rev. **D70**, 094034 (2004).

[17] K. Langfeld and L. Moyaerts, Phys. Rev. **D70**, 074507 (2004).

[18] A. P. Szczepaniak and E. S. Swanson, Phys. Rev. **D65**, 025012 (2002).

[19] S. L. Adler and A. C. Davis, Nucl. Phys. **B244**, 469 (1984).

[20] D. Alde et al., Phys. Lett. **B205**, 397 (1988).

[21] D. R. Thompson et al., Phys. Rev. Lett. **79**, 1630 (1997).

[22] S. U. Chung et al., Phys. Rev. **D60**, 092001 (1999).

[23] G. S. Adams et al., Phys. Rev. Lett. **81**, 5760 (1998).

[24] S. U. Chung et al., Phys. Rev. **D65**, 072001 (2002).

[25] A. R. Dzierba et al., Phys. Rev. **D73**, 072001 (2006).

[26] D. V. Amelin et al., Phys. Lett. **B356**, 595 (1995).

[27] A. Zaitsev, AIP Conf. Proc. **432**, 461 (1998).

[28] A. Donnachie and Y. S. Kalashnikova, Phys. Rev. **D60**, 114011 (1999).

[29] K. Karch et al., Z. Phys. **C54**, 33 (1992).

[30] J. Adomeit et al., Z. Phys. **C71**, 227 (1996).

[31] D. Barberis et al., Phys. Lett. **B413**, 217 (1997).

[32] Y. S. Kalashnikova, Null. Phys. **A689**, 49 (2001).

[33] F. Buisseret and V. Mathieu, hep-ph/0607083 (2006).

[34] C. W. Bernard et al., Phys. Rev. **D56**, 7039 (1997).

[35] C. McNeile et al., Nucl. Phys. Proc. Suppl. **73**, 264 (1999).

[36] P. Lacock and K. Schilling, Nucl. Phys. Proc. Suppl. **73**, 261 (1999).

[37] J. N. Hedditch et al., Phys. Rev. **D72**, 114507 (2005).

[38] X.-Q. Luo and Z.-H. Mei, Nucl. Phys. Proc. Suppl. **119**, 263 (2003).

[39] T. Barnes, F. E. Close, and E. S. Swanson, Phys. Rev. **D52**, 5242 (1995).

[40] F. E. Close and P. R. Page, Nucl. Phys. **B443**, 233 (1995).

[41] K. Waidelich, Spin splittings for heavy hybrid mesons, Master's thesis, North Carolina State University, 2001.

[42] T. Barnes, PhD thesis, Caltech, 1977.

[43] F. Iddir and L. Semlala, (2005).

[44] Y. Liu and X.-Q. Luo, Phys. Rev. **D73**, 054510 (2006).

[45] L. A. Griffiths, C. Michael, and P. E. L. Rakow, Phys. Lett. **B129**, 351 (1983).

[46] S. Perantonis and C. Michael, Nucl. Phys. **B347**, 854 (1990).

[47] G. P. Lepage, Journal of Comput. Phys. **27** (1978).

[48] W. M. Yao et al., J. Phys. **G33**, 1 (2006).

[49] S. J. Brodsky and G. R. Farrar, Phys. Rev. Lett. **31**, 1153 (1973).

[50] J. F. Gunion, Phys. Lett. **B88**, 150 (1979).

[51] G. T. Bodwin, E. Braaten, and J. Lee, Phys. Rev. **D72**, 014004 (2005).

[52] L. Maiani, F. Piccinini, A. D. Polosa, and V. Riquer, AIP Conf. Proc. **814**, 508 (2006).

[53] E. S. Swanson, Phys. Rept. **429**, 243 (2006).

[54] C. Quigg, PoS **HEP2005**, 400 (2006).

[55] A. P. Szczepaniak, Phys. Rev. **D69**, 074031 (2004).

Appendix

Appendix A

Color Representations

The color matrices used in the tetra-quark wavefunction are different for each color scheme. Here is a list of the possibilities:

$$|\Psi\rangle^{color} = \begin{cases} \delta_{i_1 i_2}\delta_{i_3 i_4} B^\dagger_{i_1} D^\dagger_{i_2} B^\dagger_{i_3} D^\dagger_{i_4} & \text{singlet,} \\ T^a_{i_1 i_2} T^a_{i_3 i_4} B^\dagger_{i_1} D^\dagger_{i_2} B^\dagger_{i_3} D^\dagger_{i_4} & \text{octet,} \\ {}^{(3)}T^a_{i_1 i_3}\, {}^{(3)}T^a_{i_2 i_4} B^\dagger_{i_1} B^\dagger_{i_3} D^\dagger_{i_2} D^\dagger_{i_4} & \text{triplet,} \\ {}^{(6)}T^a_{i_1 i_3}\, {}^{(6)}T^a_{i_2 i_4} B^\dagger_{i_1} B^\dagger_{i_3} D^\dagger_{i_2} D^\dagger_{i_4} & \text{sextet.} \end{cases}$$

To express the color matrices, the following auxiliary matrices are used:

$$M^1 = \frac{1}{2}\begin{pmatrix} 0 & 1 & 0 \\ 1 & 0 & 0 \\ 0 & 0 & 0 \end{pmatrix}, M^2 = \frac{1}{2}\begin{pmatrix} 0 & -i & 0 \\ i & 0 & 0 \\ 0 & 0 & 0 \end{pmatrix}, M^3 = \frac{1}{2}\begin{pmatrix} 1 & 0 & 0 \\ 0 & -1 & 0 \\ 0 & 0 & 0 \end{pmatrix},$$

$$M^4 = \frac{1}{2}\begin{pmatrix} 0 & 0 & 1 \\ 0 & 0 & 0 \\ 1 & 0 & 0 \end{pmatrix}, M^5 = \frac{1}{2}\begin{pmatrix} 0 & 0 & -i \\ 0 & 0 & 0 \\ i & 0 & 0 \end{pmatrix}, M^6 = \frac{1}{2}\begin{pmatrix} 0 & 0 & 0 \\ 0 & 0 & 1 \\ 0 & 1 & 0 \end{pmatrix},$$

$$M^7 = \frac{1}{2}\begin{pmatrix} 0 & 0 & 0 \\ 0 & 0 & -i \\ 0 & i & 0 \end{pmatrix}, M^8 = \frac{1}{2\sqrt{3}}\begin{pmatrix} 1 & 0 & 0 \\ 0 & 1 & 0 \\ 0 & 0 & -2 \end{pmatrix}, M^9 = \frac{1}{\sqrt{6}}\begin{pmatrix} 1 & 0 & 0 \\ 0 & 1 & 0 \\ 0 & 0 & 1 \end{pmatrix}.$$

Then, the color matrices are:

- **singlet:** $\delta = M^9 =$ Kronecker delta matrix;
- **octet:** $T^a = M^a = \frac{1}{2}$ Gell-Mann matrices $(a = 1, \ldots, 8)$;
- **triplet:** ${}^{(3)}T^a = M^a$ $(a = 2, 5, 7)$;
- **sextet:** ${}^{(6)}T^a = M^a$ $(a = 1, 3, 4, 6, 8, 9)$.